The impact of CO on secondary organic aerosols formed from the mixture of α-pinene and n-dodecane

Guangzhao Xie[1], Aristeidis Voliotis[1,2], Thomas J. Bannan[1], Yunqi Shao[1], Huihui Wu[1*], Dawei Hu[1,2], and Gordon McFiggans[1]

[1]Centre for Atmospheric Science, Department of Earth and Environmental Sciences, School of Natural Sciences, University of Manchester, Manchester, M13 9PL, UK

[2]National Centre for Atmospheric Science (NCAS), University of Manchester, Manchester, M13 9PL, UK

*Now at: Univ Paris Est Créteil and Université Paris Cité, CNRS, LISA, 94010 Créteil, France

Correspondence to: Gordon McFiggans (g.mcfiggans@manchester.ac.uk) and Aristeidis Voliotis (aristeidis.voliotis@manchester.ac.uk)

Abstract. ~~Atmospheric simulation chambers are powerful tools for investigating~~Secondary organic aerosol (SOA) formation is strongly influenced by atmospheric ~~processes and form the basis for model parameterisations. Ensuring the~~conditions. Achieving atmospheric relevance ~~of experimental conditions is crucial~~in chamber experiments is essential for understanding and predicting the impacts of ~~secondary organic aerosols (~~SOA~~)~~ on air quality and climate. However, many chamber studies are ~~often~~ conducted under simplified conditions~~, which may limit their applicability to real-world scenarios.~~ or with a single SOA precursor. Here, we investigated the impact of CO on ~~the~~SOA particle mass yields and chemical composition ~~of SOA particles formed~~ from α-pinene (a biogenic volatile organic compound ~~(~~, VOC~~, α-pinene), ~~), n-dodecane (an anthropogenic intermediate-volatility organic compound ~~(~~, IVOC~~, n-dodecane~~), and their mixture in the presence of nitrogen oxides (NO_x = NO + NO_2 ~~+ NO~~) in the Manchester Aerosol Chamber (MAC~~). This photochemical system better represents polluted atmospheric conditions~~) using online measurements. The results show that the influence of CO differed between single- and mixed-precursor systems. In the single-precursor systems, CO significantly suppressed SOA particle mass yields, whereas no such suppression was observed in the mixture. Moreover, compared with the single-precursor systems, CO exerted a diminished impact on the organic peroxy (RO_2) radical reaction pathways in the mixture, with the extent of this change differing between α-pinene and n-dodecane. These findings ~~demonstrate that variations in reaction conditions can lead to different responses in SOA particle properties between the single- and mixed-precursor systems, highlighting~~highlight the importance of ~~conducting~~ accounting for atmospheric complexity in laboratory ~~experiments under atmospherically relevant conditions~~studies.

1 Introduction

~~Organic aerosols (OA) account for 20 to 90% of the total atmospheric fine particulate matter mass~~Secondary organic aerosol (SOA) constitutes a substantial fraction of ambient aerosol and ~~can significantly influence climate,~~ has significant impacts on air quality, climate and human health~~. A substantial fraction of OA consists of secondary organic aerosols (SOA), which are .~~ It is formed through the ~~vapour phase~~ oxidation of gas-phase organic compounds ~~and subsequent~~followed by gas-particle partitioning (Atkinson and Arey, 2003; Hallquist et al., 2009; Jimenez et al., 2009; Ramanathan et al., 2001; Robinson et al., 2007)~~into the condensed phase~~. These processes are complex and strongly influenced by atmospheric conditions (Hallquist et al., 2009; Kroll and Seinfeld, 2008; Xu et al., 2015)~~. Comprehensive~~. Despite extensive research, achieving a comprehensive understanding and accurate prediction of SOA formation ~~are critical for assessing the impacts of aerosols on global climate and regional air quality~~remain challenging (Kenagy et al., 2024; Shrivastava et al., 2017).~~–~~

Laboratory studies and atmospheric modelling are two key approaches for investigating atmospheric SOA (Burkholder et al., 2017). Model parameterisations are largely derived from laboratory studies~~-~~, and the accuracy of model predictions strongly depends on the atmospheric relevance of experimental conditions employed (Burkholder et al., 2017; Kanakidou et al., 2005; Kenagy et al., 2024). The ambient atmosphere comprises a complex mixture of biogenic and anthropogenic emissions, including a wide range of gas-phase organic compounds and inorganic trace gases (Gu et al., 2021; Guenther et al., 1995). Field measurements have provided evidence that anthropogenic emissions can modulate SOA formed from biogenic precursors (Budisulistiorini et al., 2015; Shilling et al., 2013; Xu et al., 2015). However, many laboratory experiments are conducted under simplified ~~rather than atmospherically relevant~~ conditions ~~for experimental reasons~~or with a single SOA precursor, which may introduce uncertainties ~~in predicting SOA concentrations in~~when extrapolating these results to atmospheric models (Kenagy et al., 2024; Shrivastava et al., 2017; Tsigaridis et al., 2014).

Organic peroxy radicals (RO_2) play a central role in SOA formation (Kroll and Seinfeld, 2008; Ziemann and Atkinson, 2012). They can undergo bimolecular termination reactions with hydroperoxyl radicals (HO_2), other RO_2 radicals, or nitrogen oxides (NO_x = NO + NO_2), as well as unimolecular termination (Atkinson, 2000; Goldman et al., 2021; Molteni et al., 2019; Ziemann and Atkinson, 2012). Recent studies have focused on the autoxidation pathways of RO_2 radicals that produce highly oxygenated molecules (HOMs), which are considered potentially important contributors to SOA formation owing to their extremely low volatility (Bianchi et al., 2019; Ehn et al., 2014; Pospisilova et al., 2020). In real atmospheric environments, the coexistence of multiple SOA precursors and various inorganic trace gases introduces additional chemical complexity into the system (McFiggans et al., 2019; Xu et al., 2015)~~The ambient atmosphere comprises a complex mixture of biogenic and anthropogenic gas phase organic compounds . However, laboratory studies often focus on single precursors. Increasing evidence indicates that interactions among oxidation products from different sources can influence the formation of SOA. observed enhanced SOA production when anthropogenic emissions from Sacramento mixed with isoprene rich air from the foothills.~~. Such complexity can substantially modify RO_2 reaction pathways, thereby influencing product distributions and yields.

An increasing number of studies have focused on mixtures of multiple precursors. McFiggans et al. (2019) demonstrated that ~~the presence of isoprene can suppress the particle mass yield of SOA formed from α-pinene. In~~mixing α-pinene with isoprene substantially suppresses SOA formation from α-pinene, reducing SOA mass formation by about 60 % and SOA yield by 40 %. This suppression was attributed to two main mechanisms. First, isoprene, which exhibits a relatively low yield, efficiently competes with α-pinene for available OH, thereby suppressing the formation of α-pinene-derived RO_2 radicals. Second, isoprene-derived RO_2 radicals can scavenge HOM-RO_2 derived from α-pinene, leading to the formation of products with higher volatility. More broadly, mixing effects on SOA particle mass yields have also been observed for other precursor combinations. For example, in multi-precursor systems consisting of two monoterpenes (α-pinene and limonene), SOA formation from α-pinene was enhanced by approximately 50 %, while that from limonene was reduced by about 20 % (Takeuchi et al., 2022). More recent studies have extended such investigations to ternary mixtures comprising biogenic (α-pinene and isoprene) and anthropogenic (o-cresol) precursors, and have also shown that the overall SOA particle mass yields in the mixture deviate from those predicted by additive calculations (Voliotis et al., 2022a). These findings suggest that simple linear ~~combinations~~addition of SOA particle mass yields from individual components may lead to inaccurate estimates of total SOA formation in mixed-precursor systems.

Atmospheric inorganic trace gases, such as CO and ~~nitrogen oxides (~~NO_x ~~= NO_2 + NO),~~ can ~~influence the~~ alter oxidant levels and ~~alter the~~RO_2 reaction pathways (Atkinson, 2000; Baker et al., 2024; Chen et al., 2022; Kang et al., 2025; Kroll and Seinfeld, 2008; Lane et al., 2008; Pullinen et al., 2020; Pye et al., 2019; Sarrafzadeh et al., 2016)~~of organic peroxy (RO_2) radicals, which play a central role in the formation of SOA .~~. In laboratory ~~studies, without adequately considering the effects of these trace gases, the fate of RO_2 radicals may differ substantially from that in the real~~experiments, SOA precursor concentrations are often higher than those typically observed in the ambient atmosphere for practical reasons (Ziemann and Atkinson, 2012). This can lead to relatively low HO_2/RO_2 ratios compared with atmospheric conditions, favouring $RO_2 + RO_2$ reactions over $RO_2 + HO_2$ reactions (Ziemann and Atkinson, 2012). The former forms accretion products, which may have extremely low volatility and are expected to contribute to SOA formation, potentially leading to an overestimation of SOA particle mass yields (Kenagy et al., 2024; Peräkylä et al., 2023; Ziemann and Atkinson, 2012). The presence of CO can directly consume OH and ~~shift~~produce HO_2 radicals, thereby shifting the ~~hydroperoxy (~~HO_2~~) radical~~/RO_2 ratio~~, thereby favouring~~ and increasing the importance of the RO_2 termination ~~of RO_2 + HO_2 over RO_2 + RO_2 reactions~~via HO_2 (Lu and Khalil, 1993). Previous studies have quantified the effect of CO on SOA production. McFiggans et al. (2019) showed that CO suppressed α-pinene dimer (containing 17 to 20 carbon atoms) formation by a factor of two~~. Similarly,~~, while the amounts of HOMs were suppressed by factors of 4 to 5. Baker et al. (2024) ~~introduced CO into the α-pinene oxidation system and~~ further demonstrated that ~~unrealistically low HO_2/RO_2 ratios can lead to significant overestimation of SOA mass yields. Under elevated HO_2/RO_2-~~, under constant OH conditions, the ~~formation of highly oxygenated molecule (HOM)~~ addition of CO increased the HO_2/RO_2 ratio from approximately 1/100 to about 1/1, leading to a ~ 60 % reduction in the abundance of HOM-accretion products ~~decreased by about 60 % .~~and a ~ 30 % decrease in the SOA formation potential of HOMs. However, these studies were conducted under NO_x-free conditions. In the ambient atmosphere, ~~CO is~~high concentrations of CO are often co-emitted with other anthropogenic pollutants, such as NO_x~~, and the termination of RO_2 radicals involves complex interactions among RO_2~~, NO_x can react with RO_x radicals (RO_x = OH + HO_2 + RO_2), thereby influencing RO_x cycling and, consequently, the formation of SOA and O_3

(Chen et al., 2022; Clapp and Jenkin, 2001; Pusede et al., 2015)~~, and HO_2. It is therefore important to consider the effects of CO and NO_x in conjunction. NO_x governs O_3 concentrations through the photostationary state, thereby indirectly modulating OH via O_3 photolysis. Under NO_x free conditions, RO_2 + RO_2 and/or RO_2 + HO_2 reactions dominate over RO_2 + NO reactions, whereas in the presence of NO_x,~~. RO_2 radicals ~~can~~ react rapidly with NO to form alkoxy ~~(RO)~~ radicals (RO) or organic nitrates (Atkinson, 2000; Chen et al., 2022; Kang et al., 2025; Ziemann and Atkinson, 2012)~~($RONO_2$)~~. RO_2 can also react with NO_2 to form peroxynitrates; however, these species are generally thermally unstable, except at very low temperatures or when derived from acylperoxy radicals (Atkinson, 2000; Goldman et al., 2021; Ziemann and Atkinson, 2012)~~ observed that, in the presence of NO_x, the~~. The effects of NO_x on SOA particle mass yields have been extensively studied. Sarrafzadeh et al. (2016)~~yield of α pinene decreased significantly from 40 % to 6.6 %.~~ reported that, in β-pinene photooxidation experiments under low-NO_x conditions, SOA particle mass yields increased with rising NO_x concentrations, which they attributed to enhanced OH concentrations. However, after removing the effect of OH, the yields decreased with increasing NO_x. Pullinen et al. (2020) revealed that ~~increasing~~higher NO_x concentrations ~~led to a decrease in~~ reduced the ~~fraction~~formation of gas-phase α-pinene HOM-accretion products~~.~~, leading to a lower SOA particle mass yield. When CO and NO_x coexist, oxidant levels and RO_2 reaction pathways are influenced by multiple interacting processes. These ~~findings highlight~~ interactions contribute to the ~~need for laboratory studies to account for~~ complexity of the ~~full range of atmospherically relevant conditions~~ambient atmosphere. It is therefore important to investigate SOA formation in systems containing multiple trace gases.

In this study, we employed a photochemical system incorporating mixtures of biogenic and anthropogenic SOA precursors together with multiple inorganic trace gases commonly associated with anthropogenic emissions. Within this framework, we investigated the impact of CO on ~~the~~SOA particle mass yields and chemical composition ~~of SOA particles formed~~ from ~~a biogenic volatile organic compound (VOC,~~ α-pinene~~), an anthropogenic intermediate-volatility organic compound (IVOC~~, n-dodecane~~),~~, and their mixture~~,~~ in the presence of NO_x. Based on changes in chemical composition, we inferred shifts in RO_2 reaction pathways and their potential influence on yields. α-Pinene ($C_{10}H_{16}$) is the most abundant monoterpene in the troposphere and contributes significantly to the global SOA budget (Andreae and Crutzen, 1997; Lee et al., 2006). n-Dodecane ($C_{12}H_{26}$) serves as a proxy for anthropogenic ~~IVOCs,~~intermediate-volatility organic compounds (IVOCs), being widely present in fuels and emitted primarily as a non-combusted hydrocarbon (Zhao et al., 2015). ~~CO and NO_x are ubiquitous atmospheric trace gases with substantial anthropogenic sources.~~ Experiments were conducted in the Manchester Aerosol Chamber (MAC), using ~~a combination of~~ online ~~and offline~~ instruments to characterise particle- and gas-phase compounds. ~~This work provides new insights into SOA particle properties under polluted conditions more representative of the atmosphere.~~

Table 1. Summary of experimental conditions.

Experiment No.	Experiment Type	$[\text{n-dodecane}]_0$[a] (ppb)	$[\alpha\text{-pinene}]_0$[a] (ppb)	$[NO_x]_0$[a] (ppb)	$[\text{precursor}]_0$[a] $/[NO_x]_0$	$[CO]_0$[a] (ppb)	$[\text{Seed}]_0$[a] (μg m^{-3})	$[O_3]_{max}$ (ppb)	SOA (μg m^{-3})	SOA particle mass yields
α-Pinene experiments										
1	α-pinene	-	59.4	57	1.0	171	31.0	37.9	39.9	0.12
2	α-pinene	-	48.9	54	0.9	185	56.1	39.0	42.1	0.16
3	α-pinene + CO	-	42.7	68	0.6	8360	35.9	60.7	17.8	0.08
n-Dodecane experiments										
4	n-dodecane	160	-	281	0.6	160	37.8	103.1	177.5	N.A.[b]
5	n-dodecane	160	-	156	1.0	195	31.2	98.4	122.9	0.17
6	n-dodecane + CO	160	-	133	1.2	9261	48.2	99.1	26.3	0.05
7	n-dodecane + CO	160	-	204	0.8	9473	47.1	98.5	14.7	0.02
Mixed-precursor experiments										
8	mixture	80	24.8	160	0.9	139	34.5	85.9	71.4	N.A.[b]
9	mixture	80	27.4	121	0.6	168	36.9	76.2	63.9	0.11
10	mixture + CO	80	22.1	109	0.6	10000	45.6	93.8	67.1	0.18
11	mixture + CO	80	14.3	161	0.9	10668	37.8	109.4	50.5	0.14

[a] The subscript "0" indicates the initial concentration.

[b] N.A.: no available data.

2 Methodology

2.1 Generic peroxy radical chemistry

The analysis has been informed by the prevailing generic peroxy radical chemistry. RO_2 radicals can undergo bimolecular termination reactions with HO_2 radicals, other RO_2 radicals, or NO_x, leading to the formation of closed-shell products (Atkinson, 2000; Ziemann and Atkinson, 2012).

Hydroperoxides:

$$RO_2 + HO_2 \rightarrow ROOH + O_2 \quad \text{R1}$$

Carbonyls and alcohols:

$$RO_2 + RO_2 \rightarrow R{=}O + ROH + O_2 \quad \text{R2}$$

Organic nitrates:

$$RO_2 + NO \rightarrow RONO_2 \quad \text{R3}$$

Peroxynitrates:

$$RO_2 + NO_2 \rightarrow RO_2NO_2 \quad \text{R4}$$

Accretion products:

$$RO_2 + RO_2 \rightarrow ROOR + O_2 \quad \text{R5}$$

RO_2 radicals can also undergo unimolecular reactions that lead to the formation of carbonyls (Goldman et al., 2021; Molteni et al., 2019).

$$RO_2 \rightarrow QOOH;\ QOOH + O_2 \rightarrow O_2QOOH;\ O_2QOOH \rightarrow HO_2Q{=}O + OH \quad \text{R6}$$

QOOH is a key oxidation intermediate formed via intramolecular hydrogen abstraction by RO_2 radicals.

Besides closed-shell products, RO_2 radicals can also form RO radicals (Orlando et al., 2003).

$$RO_2 + NO \rightarrow RO + NO_2 \quad \text{R7}$$

$$RO_2 + RO_2 \rightarrow RO + RO + O_2 \quad \text{R8}$$

$$RO_2 + HO_2 \rightarrow RO + OH + O_2 \quad \text{R9}$$

HOMs are formed via autoxidation pathways of RO_2 radicals (Bianchi et al., 2019; Goldman et al., 2021).

$$RO_2 \rightarrow QOOH;\ QOOH + O_2 \rightarrow O_2QOOH \quad \text{R10}$$

These reaction pathways compete with one another, thereby influencing the distribution of products.

α-Pinene photooxidation is expected to produce $C_{10}H_{15}O_x$ and $C_{10}H_{17}O_x$ as major RO_2 families. The $C_{10}H_{17}O_x$ family is initiated via OH addition to α-pinene (Berndt et al., 2016; Jenkin et al., 1997; Kang et al., 2025; Vereecken and Peeters, 2004). RO_2 + HO_2 termination (R1) of $C_{10}H_{17}O_x$ forms $C_{10}H_{18}O_n$ hydroperoxides, and RO_2 + RO_2 termination (R2) yields $C_{10}H_{16}O_n$ carbonyls and $C_{10}H_{18}O_n$ alcohols. Unimolecular termination (R6) of $C_{10}H_{17}O_x$ generates $C_{10}H_{16}O_n$ carbonyls. The $C_{10}H_{15}O_x$ family is formed via hydrogen abstraction from α-pinene or from first-generation oxidation products (e.g., pinonaldehyde), as

well as directly from ozonolysis through the vinyl hydroperoxide pathway (Jenkin et al., 1997; Johnson and Marston, 2008; Kang et al., 2025). $RO_2 + HO_2$ termination (R1) of $C_{10}H_{15}O_x$ forms $C_{10}H_{16}O_n$ hydroperoxides, whereas $RO_2 + RO_2$ termination (R2) produces $C_{10}H_{14}O_n$ carbonyls and $C_{10}H_{16}O_n$ alcohols. Unimolecular termination (R6) of $C_{10}H_{15}O_x$ generates $C_{10}H_{14}O_n$ carbonyls. $RO_2 + RO_2$ reactions (R2) between $C_{10}H_{15}O_x$ and $C_{10}H_{17}O_x$ radicals lead to the formation of $C_{10}H_{14}O_n$ carbonyls and $C_{10}H_{18}O_n$ alcohols, and/or $C_{10}H_{16}O_n$ carbonyls and alcohols.

The main RO_2 radicals expected from n-dodecane photooxidation are $C_{12}H_{25}O_x$ family (Zhang et al., 2014). $RO_2 + HO_2$ termination (R1) yields $C_{12}H_{26}O_n$ hydroperoxides, while $RO_2 + RO_2$ termination (R2) produces $C_{12}H_{24}O_n$ carbonyls and $C_{12}H_{26}O_n$ alcohols. Unimolecular termination (R6) of $C_{12}H_{25}O_x$ generates $C_{12}H_{24}O_n$ carbonyls.

In the mixture, RO_2 radicals originating from different precursors can undergo cross-reactions. Reactions (R2) between $C_{10}H_{15}O_x$ and $C_{12}H_{25}O_x$ yield $C_{10}H_{14}O_n$ carbonyls and $C_{12}H_{26}O_n$ alcohols or $C_{12}H_{24}O_n$ carbonyls and $C_{10}H_{16}O_n$ alcohols. Similarly, reactions (R2) between $C_{10}H_{17}O_x$ and $C_{12}H_{25}O_x$ lead to the formation of $C_{10}H_{16}O_n$ carbonyls and $C_{12}H_{26}O_n$ alcohols, or $C_{12}H_{24}O_n$ carbonyls and $C_{10}H_{18}O_n$ alcohols.

RO radicals formed via reactions R7–R9 can subsequently undergo unimolecular decomposition, isomerisation, or react with O_2 (Orlando et al., 2003). Reaction of RO radicals with O_2 leads to the formation of carbonyl compounds and HO_2 radicals:

$$RO + O_2 \rightarrow R'CHO + HO_2 \qquad \text{R11}$$

RO radicals derived from $C_{10}H_{15}O_x$ can form $C_{10}H_{14}O_n$ carbonyls via this pathway, whereas RO radicals derived from $C_{12}H_{25}O_x$ yield $C_{12}H_{24}O_n$ carbonyls.

Theoretically, $C_{10}H_{14}O_n$ and $C_{12}H_{24}O_n$ carbonyls can be formed via multiple pathways, including $RO_2 + RO_2$ reactions (R2), unimolecular termination of RO_2 radicals (R6), and reaction of RO radicals with O_2 (R11). However, previous studies have demonstrated that, under ambient-temperature conditions and in the presence of NO_x, unimolecular termination pathways are not expected to be dominant in RO_2 chemistry (Goldman et al., 2021; Goss et al., 2025). In addition, RO radicals derived from α-pinene generally favour fragmentation owing to the low energy barrier for C-C bond scission (Dibble, 2001). For linear RO radicals formed from long-chain alkanes, isomerisation dominates over reactions with O_2 (Atkinson, 2007; Ziemann and Atkinson, 2012)~~2.1~~. On this basis, both unimolecular termination and RO + O_2 reactions are expected to make only minor contributions and are therefore not explicitly considered in this study.

Therefore, $C_{10}H_{14}O_n$ and $C_{12}H_{24}O_n$ carbonyls are expected to be formed predominantly via $RO_2 + RO_2$ reactions (R2). In contrast, $C_{10}H_{16}O_n$, $C_{10}H_{18}O_n$, and $C_{12}H_{26}O_n$ species can be produced not only through reactions (R2) but also via $RO_2 + HO_2$ pathways (R1). Accordingly, changes in the relative abundances of $C_{10}H_{14}O_n$ and $C_{12}H_{24}O_n$ compounds are used as indicators to assess the influence of CO on RO_2 chemistry. In general, the presence of CO is expected to reduce the relative contribution of $RO_2 + RO_2$ termination, which would be reflected in decreased relative abundances of $C_{10}H_{14}O_n$ and $C_{12}H_{24}O_n$ species.

2.2 Experimental setup and procedure

The experiments were conducted in the 18 m^3 MAC at the University of Manchester. The chamber comprises a fluorinated ethylene propylene (FEP) Teflon bag supported by three rectangular frames. Further details of the chamber are provided in Shao et al. (2022). Illumination was provided by a series of halogen lamps (50W/4700K MR16, Solux),. The irradiation source, consisting of two xenon arc lamps (XBO 6000W/HSLA OFR, Osram),) and a series of halogen lamps (50W/4700K MR16, Solux), is mounted inside the chamber and generates irradiation over the wavelength range of 290–800 nm to mimic the atmospheric radiation spectrum. The corresponding actinic flux spectrum is presented in Shao et al. (2022). The photolysis rate of NO_2 (J_{NO_2}) was 1.38 × 10^{-3} s^{-1}. To promote OH radical production, an additional UVC lamp operating at 254 nm.(TUV 130W XPT SE UNP/20, Philips) was installed, with more than 90 % of its length masked to prevent excessive irradiation. The liquid precursors (α-pinene, analyticanalytical standard, Sigma-Aldrich; n-dodecane, anhydrous, ≥ 99.0 %, Sigma-Aldrich) were initially injected via syringe into a heated glass bulb to facilitate vaporisation. The resulting, after which the vapours were subsequently carried into the chamber by electronic capture device-grade nitrogen (ECD N_2). NO_x was introduced from a custom-made cylinder using ECD N_2 as the carrier gas. TheyNO_2 served as athe source of OH viaO_3, and the subsequent O_3 photolysis generated OH radicals, thereby initiating the photochemical oxidation. The initial precursor/NO_x ratios were controlled within the range of 0.6 to1to 1.2, while the initial NO_2/NO ratios were maintainedranged between 1.5 and 2.5. Seed particles with a mass concentration of 40.2 ± 8.0 μg m^{-3} were generated by nebulising aqueous ammonium sulfate solutions ($(NH_4)_2SO_4$, ACS reagent, ≥ 99.0 %, Sigma-Aldrich) using an aerosol generator. (ATM 230, Topas). During seed injection, the carrier air was passed through the humidifier, ensuring the deliquescence of the seeds as they were generated. These particles provided a condensation surface for the oxidation products, thereby reducing wall losses and suppressing nucleation (Nah et al., 2017).

The initial experimental conditions are summarised in Table 1. Each experiment typically consisted of four steps (Fig. S1):.

(i) Pre-experiment: Prior to each run, a series of preparation steps Repeated flush-fill cycles were conducted, including cyclic flushing to achieve a low-background condition. During these cycles, the chamber was flushed for approximately 7 min and fillingthen refilled with clean air at a highthe same flow rate, with this procedure repeated for approximatelyabout 1.5 h, preheating the precursor injection bulb, introducing all reactants. Subsequently, SOA precursors, NO_x, CO, and seed aerosols, and adjusting were introduced into the chamber. The temperature and relative humidity were adjusted to the target values (approximately 25 °C°C and 50 ± 5 %, respectively).

(ii) Stabilisation: The chamber was kept in the dark for 20 to 30 min with all the reactants and seed aerosols, allowing their concentrations to stabilise. initial conditions prior to illumination.

(iii) Experiment: Each photochemical experiment lasted for approximately 5 h, corresponding to four cycles of the Filter Inlet for Gases and Aerosols coupled to a Chemical Ionisation Time-of-Flight Mass Spectrometer (FIGAERO-CIMS). Each cycle spanned 1.5 h, with the first 30 min allocated to gas and particle sampling and gas-phase analysis, followed by 1 h of particle-phase analysis (described in Sect. 2.3.1). In the final cycle, the photochemical reaction was terminated after the completion of particle samplingWhen the lights were turned on, photooxidation and subsequent SOA formation were initiated. Each "experiment" phase lasted for approximately 5 h.

(iv) Post-experiment: After the ~~light sources~~lights were ~~switched~~turned off, the chamber underwent ~~cyclic flushing and filling with clean air~~repeated flush-fill cycles for approximately 1 h. It was then filled with ~~ozone~~O_3 at a high concentration (≥ 1 ppm) and left to soak overnight to oxidise and remove residual O_3-~~reacting~~reactive organic species.

~~Table 1 summarises the key experimental conditions and results. Repeat experiments were conducted to enhance the reliability of the results and to address data gaps caused by instrument failures. Instrument availability for each experiment is listed in Table S1. Unless otherwise stated, the figures in this paper show mean values from the available repeat experiments.~~

2.~~2~~3 Iso-reactivity conditions

OH radicals served as the primary oxidant in our experiments. ~~To ensure comparability across systems, all~~All experiments were initiated ~~with~~under iso-reactivity ~~towards OH radicals~~conditions with respect to OH (Voliotis et al., 2022b; Voliotis et al., 2021). Specifically, the total OH reactivity was kept constant between single- and mixed-precursor systems. In the ~~mixture, the~~mixed-precursor system, SOA precursor concentrations were ~~adjusted to contribute~~set such that each contributed equally to the ~~overall~~total OH reactivity. ~~This approach ensured that both precursors~~Under these conditions, each precursor had an equal initial probability of reacting with OH and producing first-generation oxidation products (Voliotis et al., 2022b; Voliotis et al., 2021). The initial reactivity was calculated using the following equation:

$$\text{Initial reactivity } (s^{-1}) = \sum C_{precursor,i} \times K_{OH,i} \quad (1)$$

where $C_{precursor,i}$ is the concentration of precursor i (molecule cm^{-3}), and $k_{OH,i}$ is the reaction rate coefficient of precursor i with OH (cm^3 $molecule^{-1}$ s^{-1}). The reaction rate coefficients for α-pinene and n-dodecane with OH are 5.33×10^{-11} and 1.32×10^{-11} cm^3 $molecule^{-1}$ s^{-1}, respectively (Atkinson, 2003; Dash et al., 2014). As α-pinene exhibits greater reactivity towards OH than n-dodecane, a higher initial concentration of n-dodecane was used to achieve iso-reactivity in the experiments. The target mixing ratios of α-pinene were 40 ppb in the single-precursor system and 20 ppb in the mixed-precursor system, while those of n-dodecane were 160 ppb and 80 ppb, respectively. The ratio of α-pinene to n-dodecane falls within the range observed in urban and roadside environments (Okada et al., 2012). The initial CO concentration was also determined according to the principle of iso-reactivity. The reaction rate coefficient of CO with OH is 2.50×10^{-13} cm^3 $molecule^{-1}$ s^{-1} (Amedro et al., 2012).

2.~~3~~4 Instrumentation

Near-real-time gas- and particle-phase composition was measured using a Filter Inlet for Gases and Aerosols coupled to a Chemical Ionisation Time-of-Flight Mass Spectrometer (FIGAERO-CIMS~~(~~, Aerodyne Research Inc.). ~~Precursors (α-pinene and n-dodecane)~~SOA precursors were measured in real time using a Vocus Proton-Transfer Reaction Time-of-Flight Mass ~~Spectrometry~~Spectrometer (Vocus PTR-ToF-MS, Tofwerk). The non-refractory submicron aerosol particle composition, including ~~aerosol~~ sulfate, nitrate, ammonium, chloride, and organics, was measured in real time using a Compact Time-of-Flight Aerosol Mass Spectrometer (C-ToF-AMS, Aerodyne Research Inc.). NO and NO_2 were measured using a chemiluminescence NO-NO_2-NO_x analyser (Model 42i, Thermo Fisher Scientific Inc.). O_3 and CO were measured using a UV absorption O_3 analyser (Model 49C, Thermo Fisher Scientific Inc.) and a CO analyser (Model 48i, Thermo Fisher Scientific

Inc.), respectively. ~~Particle~~The mass concentration of seed aerosols in the 20–500 nm size range was measured ~~with~~using a Differential Mobility Particle Sizer (DMPS), consisting of a Vienna-design differential mobility analyser (DMA) coupled to a Condensation Particle Counter (CPC, model 3775, TSI Inc.) (Alfarra et al., 2012)~~.)~~. The availability of instruments for each experiment is listed in Table S1.

2.~~3~~4.1 FIGAERO-CIMS

The FIGAERO system enables simultaneous characterisation of gas- and particle-phase species by sampling gases through one inlet while collecting particulate matter on a filter via a separate sampling port (Bannan et al., 2019; Lopez-Hilfiker et al., 2014). The instrument was operated in negative-ion mode using I^- as the reagent ion, generated by passing CH_3I and N_2 over a ^{210}Po radioactive source. It was run in a cyclic mode consisting of the following procedure:

(i) 30 min of gas-phase sampling and simultaneous particle collection onto a PTFE filter (2.0 µm pore size, Zefluor; filters were pre-heated to 200 °C to remove potential contaminants) both at 1 L min^{-1}. During this step, the instrument was flushed with N_2 for 0.5 min every 4.5 min to obtain the gas-phase instrument background signal.

(ii) 25 min of temperature-programmed thermal desorption of the collected particles, with the temperature ramped from ambient to ~~310 °C,~~200 °C.

(iii) 15 min of isothermal soaking at ~~310 °C,~~200 °C.

(iv) 20 min of cooling from ~~310 °C~~200 °C to ambient temperature.

(v) 2 min of N_2 flushing to clean the instrument.

~~An "instrument background"~~Each cycle spanned approximately 1.5 h, and each experiment comprised four such cycles. In the final cycle, the photochemical reaction was terminated after procedure ~~was~~ (i), corresponding to the completion of particle sampling (Fig. S1).

To account for background species in the chamber, background measurements were conducted weekly ~~to correct for the~~. During these measurements, all components (SOA precursors, seed particles, CO, and NO_x) were injected under the same conditions as in the regular experiments, while the chamber was kept in the dark. Data obtained during these background measurements were subtracted from the corresponding gas- and particle-phase ~~background.~~ data acquired during the "experiment" phase.

The FIGAERO-CIMS data were analysed using the Tofware package (v4.0.0) in Igor Pro 7.0.8 (WaveMetrics©). ~~Peak~~I^-, H_2OI^-, $CH_2O_2I^-$, and I_3^- were used for mass-to-charge calibration (calibration error ≤ 3 ppm). High-resolution peak identification and fitting ~~was~~were performed ~~over~~in the m/z range of 200–550 (iodide adducts), which contained the vast majority of the total signal. Owing to the lack of available calibration standards and potential variability in instrument sensitivity across different oxygenated organic compounds, quantitative analysis using I^--CIMS remains challenging (Lee et al., 2014) ~~to 550 Da.~~. As a result, a uniform instrument sensitivity was assumed for all detected products. Additional uncertainties arise from the thermal decomposition in the FIGAERO. As shown in Fig. S2, several compounds with relatively low carbon numbers exhibited comparatively high average carbon oxidation state ($\overline{OSc}$) values and elevated maximum desorption temperature (T_{max}).

However, these species together accounted for less than 10 % of the total signal, indicating that the impact of thermal decomposition on the chemical composition was limited.

2.~~3~~4.2 Vocus PTR-ToF-MS

The Vocus PTR-ToF-MS provides high-sensitivity and fast-response measurements of organic compounds without the need for pre-concentration or chromatographic separation. Compared to traditional PTR-MS, the Vocus employs a focusing ion-molecule reactor (IMR) ~~equipped with~~ consisting of a glass tube that is mounted inside a radio frequency (RF) quadrupole, ~~which focuses ions~~ with an axial electric field applied along the ~~central axis of the reactor and thereby improves~~tube. This design enhances ion transmission efficiency and suppresses the clustering of ions with water molecules, thereby improving sensitivity and lowering the limit of detection (Jensen et al., 2023; Krechmer et al., 2018; Yuan et al., 2017). ~~An axial electric field is applied within the IMR to increase ion collision energies and suppress the clustering of ions with water molecules .~~

In our experiments, the ion source was supplied with a 20 sccm flow of water vapor. The IMR was operated at 60 °C and 2.0 mbar, with an axial voltage of approximately 568 V and an RF amplitude of 450 V at 1.3 MHz. The reduced electric field strength (E/N) was 141 Td. Measurements were ~~made~~conducted on a 5 min cycle, consisting of ~~a~~ 4 min ~~chromatography cycle and a~~of sampling followed by 1 min of instrumental background measurement. Instrument calibration was conducted daily. The calibration curve for α-pinene is presented in Fig. ~~S2~~S3. Owing to the absence of an n-dodecane ~~gas~~calibration standard, direct quantification was not feasible. Moreover, n-dodecane undergoes extensive fragmentation during ionisation, and its protonated molecular ion signal is ~~subjected~~subject to interference ~~by~~from overlapping ~~fragments~~species. Therefore, alternative approaches were adopted for its quantification: (i) the initial ~~concentrations~~mixing ratios were taken as the ~~set~~target values (160 ppb in the single-precursor system and 80 ppb in the mixed-precursor system), and (ii) the relative consumption of n-dodecane was inferred from the ~~signal changes~~temporal evolution of ~~representative~~ the $C_{10}H_{21}^+$ fragment ~~ions. In this study, the~~ ion ~~$C_{10}H_{21}^+$ was selected as a marker ion of n-dodecane to track its temporal behaviour~~ (Fig. ~~S3~~S4). However, ~~this ion may still be influenced by contributions~~interference from other oxidation products~~, which could result in~~ or fragments cannot be fully excluded and may have led to an overestimation of SOA particle mass yields. Nevertheless, this uncertainty ~~does not~~is unlikely to affect the ~~observed effects of CO on the~~ overall trends ~~and~~or relative differences in yields.

2.~~3~~4.3 C-ToF-AMS

A detailed description of the C-ToF-AMS can be found in Drewnick et al. (2009). Ionization efficiency (IE) and relative ionization efficiency (RIE) calibrations were carried out using size-selected NH_4NO_3 and $(NH_4)_2SO_4$ particles. The average IE of NH_4NO_3 was determined to be 2.75 × 10^{-7} ions molecule^{-1}, while the RIE for NH_4^+ and SO_4^{2-} were 4.71 ± 0.24 and 1.13 ± 0.01, respectively. These values are comparable to those reported in the literature (Canagaratna et al., 2007; Lannuque et al., 2023).

In this study, the organic aerosol (OA~~/~~)/sulfate correction method was applied to ~~calibrate~~correct for chamber wall losses in the SOA particle mass ~~concentration derived from~~concentrations measured by AMS ~~measurements~~ (Wang et al., 2018). This

method assumes that the loss rate constants of OA and seed aerosols are identical, and that seed concentrations are affected solely by wall loss. The corrected particle mass concentration is given by:

$$C_{OA}(t) = \frac{C_{OA}^{SUS}(t)}{C_{seed}(t)} C_{seed} \frac{C_{OA}(t)}{C_{seed}(t)} C_{seed}(0) \quad (2)$$

where $C_{OA}^{SUS}(t)/C_{seed}(t) C_{OA}(t)/C_{seed}(t)$ represents the SOA-to-sulfate ratio derived from AMS measurements, and $C_{seed}(0)$ denotes the sulfate concentration at the beginning of the experiment.

SOA particle mass yields (Y_{SOA}) for each system were derived from SOA particle mass concentrations measuremeasured by AMS and precursor concentrations measured by PTR. It is defined as the mass of SOA particles formed per unit of precursor consumed (Gao et al., 2022):

$$Y_{SOA} = \frac{\Delta SOA}{\Delta HC} \frac{\Delta SOA}{\Delta precursor} \quad (3)$$

For the single-precursor systems, ΔHC (hydrocarbon consumption$precursor$ (μg m^{-3}) denotes the consumption of the individual precursorα-pinene or n-dodecane, whereas forin the mixed-precursor system, it refers to the total consumption of all precursorsα-pinene and n-dodecane. In this study, the SOA particle mass yield refers to the overall yield and is calculated as the ratio of the total SOA particle mass formed to the total precursor consumed at the end of the experiment.

3 Results

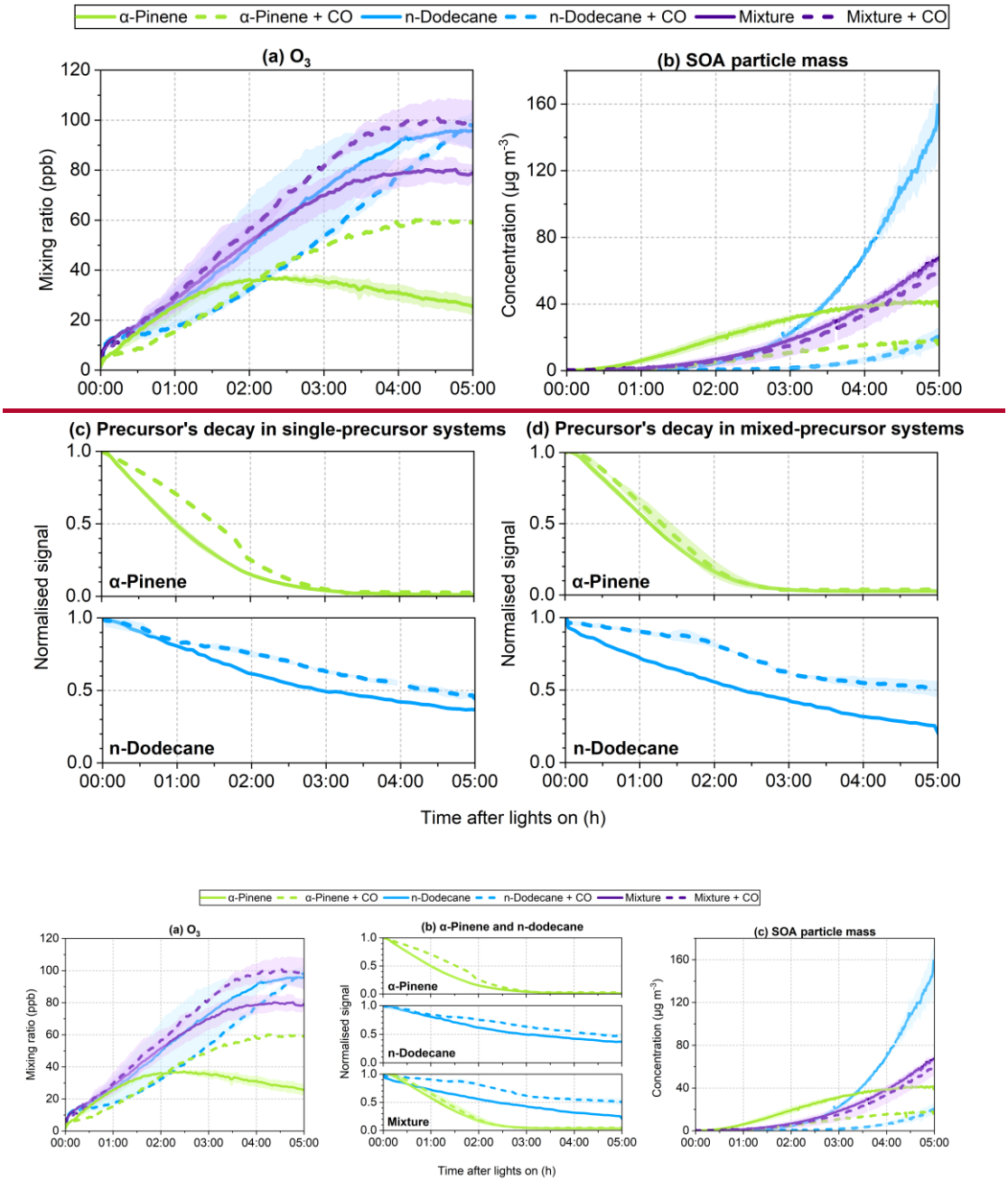

Figure 1: Time series of (a) O_3, (b) normalised SOA precursor signals, and (c) SOA particle mass concentrations~~, (c) and (d) normalised signal of the precursors~~ during the photochemical reaction of α-pinene, n-dodecane and their

mixture. Time 0 corresponds to the start of step (iii) (Sect. 2.2), when the chamber lights were turned on. Solid and dashed lines denote experiments conducted without and with CO, respectively. ~~The~~Where duplicate experiments were available, the lines represent the mean values, and the shaded area ~~represents the envelope of the measurements from repeat experiments.~~indicates the range between replicates (Table 1).

~~Fig.~~Figure 1 presents ~~an overview of~~ the temporal evolution of O_3, precursor decay, and SOA particle mass concentrations~~, and precursor decay~~ during the photochemical reactions. Solid and dashed lines represent experiments conducted in the absence and presence of CO, respectively. The corresponding time series of NO, NO_2, and CO are shown in Fig. ~~S4~~S5. These observations form the basis for evaluating the influence of CO on SOA particle formation and mass yields across different systems. Detailed results from the α-pinene, n-dodecane, and mixed-precursor experiments are presented in the following subsections.

3.1 α-Pinene

3.1.1 SOA particle mass ~~formation and~~ yields

The initial O_3 concentration in the chamber was negligible. Upon illumination, O_3 gradually accumulated, peaking at 38.5 ppb approximately two hours after lights on in the absence of CO, and then declined over time~~.~~ (Fig. 1a). In the presence of CO, the peak O_3 concentration (60.7 ppb) was observed near the end of the experiment.

The initial α-pinene/NO_x ratio in the α-pinene experiments was approximately 0.8 ~~± 0.2~~ (Table 1). In the absence of CO, NO_x concentrations declined during the first two hours of the reaction and subsequently stabilised~~, whereas~~. In contrast, in the presence of CO, ~~they~~NO_x declined continuously throughout the experiment (Fig. ~~S4~~S5). α-Pinene was ~~nearly completely~~almost entirely consumed within three hours ~~in~~under both ~~experiments~~conditions (Fig. ~~1c~~1b). Notably, ~~its~~the initial consumption rate was ~~slower~~lower in the presence of CO~~, but increased after~~. After approximately two hours~~-~~, however, the decay rate increased and ~~ultimately~~eventually converged with that observed in the absence of CO.

Compared to the experiment without CO, SOA particle mass increased more slowly in the presence of CO ~~resulted in a slower growth rate and a~~, resulting in substantially lower SOA particle mass ~~concentration~~concentrations (Fig~~1b~~. 1c). In both cases, the concentrations stabilised during the final hour of the reaction. By the end of the experiment, SOA particle mass concentrations reached 41.0 μg m^{-3} in the absence of CO and 17.8 μg m^{-3} in its presence. Correspondingly, the α-pinene SOA particle mass yield decreased from 0.14 to 0.08.

3.1.2 SOA particle chemical composition

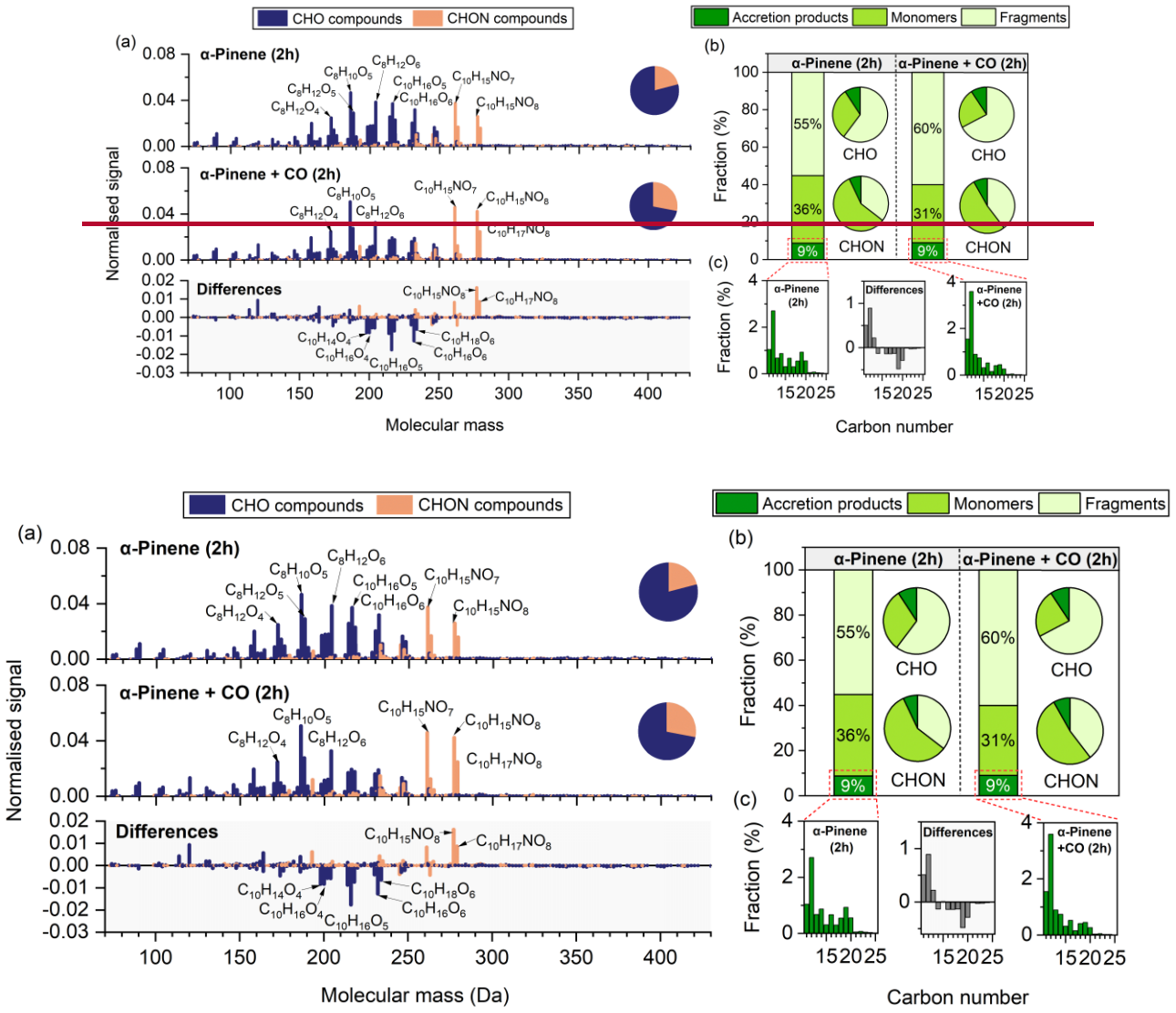

Figure 2: (a) High-resolution mass spectra of particle-phase compounds ~~identified~~measured by FIGAERO-CIMS in α-pinene experiments conducted with and without CO, ~~along with their differences~~and the corresponding difference spectra (with CO minus without CO). Prominent peaks are labelled with their corresponding molecular formulas. All signal intensities are normalised to 1. Pie charts display the proportions of CHO and CHON ~~compounds~~groups. (b) Fractions of α-pinene-derived fragments~~,~~ (C < 10), monomers~~,~~ (C = 10), and accretion products (C > 10) in the absence and presence of CO. Bar charts represent their relative contributions to the total signal, while pie charts show their ~~relative contributions~~ distribution within the CHO and CHON ~~compounds~~groups. (c) Carbon number distributions of

accretion products in the absence (left) and presence (right) of CO. The middle panel shows the differences between ~~them~~the two conditions (with CO minus without CO).

Owing to the absence of data from the final two FIGAERO cycles in the α-pinene experiment with CO, the analysis of ~~α-pinene~~ SOA particle composition was based on the second cycle, corresponding to two hours of reaction, by which time substantial SOA mass had already formed.

~~Fig.~~Figure 2a presents the high-resolution mass spectra of ~~identified SOA particles~~particle-phase compounds from α-pinene experiments conducted with and without CO, together with their differences. The products were mainly distributed within the molecular mass range of 150~~ to 280 Da. According to~~ 280 Da. Under both conditions, $C_8H_{10}O_5$ was the most abundant compound. Based on elemental composition, the compounds were classified into CHO and CHON groups. CHON species accounted for 21 % of the total signal in the absence of CO and 28 % in its presence. ~~In both cases, the most abundant compound was $C_8H_{10}O_5$.~~

The ~~identified~~ compounds can be categorised into three classes based on carbon number: monomers, fragments, and accretion products (Fig. 2b). Monomers derived from α-pinene consisted of C_{10} products~~;~~, whereas fragment compounds contained fewer than 10 carbon atoms~~, while~~ and accretion products contained more than 10. ~~Fragment compounds were the dominant class in both the absence and presence of CO,~~ Fragments dominated under both conditions, accounting for 55 % and 60 % of the total signal~~,~~ in the absence and presence of CO, respectively. ~~A large fraction of these~~Within the CHO group, fragments ~~fell within the C_7 to~~ contributed more than 60 %, with a substantial proportion distributed in the C_7–C_9 range (Fig. ~~S10). Among CHO compounds, fragments made up the largest proportion, whereas monomers dominated the CHON fraction. Notably, differences in carbon number distribution between the two systems were primarily observed~~S11). Monomers accounted for 36 % and 31 % in the ~~monomer group (Fig. S10), with~~ absence and presence of CO ~~leading~~, respectively, and were the dominant class within the CHON group, accounting for more than 50 %. The presence of CO led to a lower proportion of C_{10} CHO compounds (e.g., $C_{10}H_{16}O_{4-6}$) and a higher proportion of C_{10} CHON compounds (e.g., $C_{10}H_{15}NO_{7-8}$) ~~compared the experiment without CO~~ (Fig. 2a). The overall ~~contribution of accretion products remained consistent at 9 % in both systems. However, CO reduced the fraction of accretion products containing 16 to 24 carbon atoms compared to the experiment without~~remained constant at 9 % under both conditions. However, the proportion of C_{16}–C_{24} accretion products was lower in the presence of CO (Fig. 2c).

~~Beyond differences in carbon number distribution, the presence of CO also altered the distribution of hydrogen atom numbers (Fig. S11). Compared with the experiment without CO, CHO compounds containing 14, 16, and 18 hydrogen atoms accounted for a lower fraction in the presence of CO. In contrast, CO led to an increase in the relative abundance of CHON compounds across full range of hydrogen atom numbers detected in this study, consistent with the observed overall increase in CHON contribution.~~

The major RO_2 radicals derived from α-pinene react via the R1 and R2 pathways to form the $C_{10}H_{14}O_n$, $C_{10}H_{16}O_n$, and $C_{10}H_{18}O_n$ families. As shown in Fig. 3, in the absence of CO these species accounted for 11.0 %, 13.6 %, and 4.0 % of the CHO group, respectively, and decreased to 9.0 %, 9.5 %, and 2.4 % in its presence.

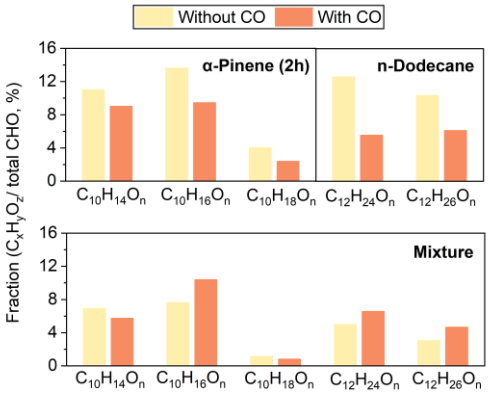

Figure 3: Relative contributions of $C_{10}H_{14}O_n$, $C_{10}H_{16}O_n$, $C_{10}H_{18}O_n$, $C_{12}H_{24}O_n$, and $C_{12}H_{26}O_n$ to the CHO group in the α-pinene, n-dodecane, and mixture systems in the absence and presence of CO.

3.2 n-Dodecane

3.2.1 SOA particle mass ~~formation and~~ yields

In the n-dodecane experiments, O_3 concentrations were generally higher in the absence of CO than in its presence (Fig. 1a). The temporal evolution of O_3 differed markedly between the two ~~systems~~conditions. In the absence of CO, O_3 had nearly reached its peak by the end of the experiment, whereas in the presence of CO~~, O_3 levels~~ it continued to ~~rise~~increase throughout the experiment. Despite these differences in formation rates and peak timing, the final O_3 concentrations in both systems converged to similar levels, approaching 100 ppb.

The initial n-dodecane/NO_x ratio was approximately 0.9 ~~± 0.3~~ (Table 1). NO_x concentrations declined steadily throughout the ~~reaction~~experiment under both conditions (Fig. ~~S4~~S5). In the presence of CO, the ~~consumption~~decay rate of n-dodecane was ~~slower~~lower (Fig. ~~1c~~1b). By the end of the experiment, 37 % of the initial n-dodecane remained unreacted in the absence of CO, whereas 47 % remained when CO was present (Fig. ~~1c~~1b).

~~The formation rate of n-dodecane SOA particles increased throughout the experiment (Fig. 1b).~~ In the absence of CO, the final SOA particle mass concentration reached 122.9 μg m^{-3} ~~of SOA particles were produced~~, corresponding to a mass yield of 0.17 (~~exp~~Exp. 5). In the presence of CO, ~~the final SOA particle mass concentration was significantly lower, at~~it reached 20.5 μg m^{-3}, with a yield of 0.04.

3.2.2 SOA particle chemical composition

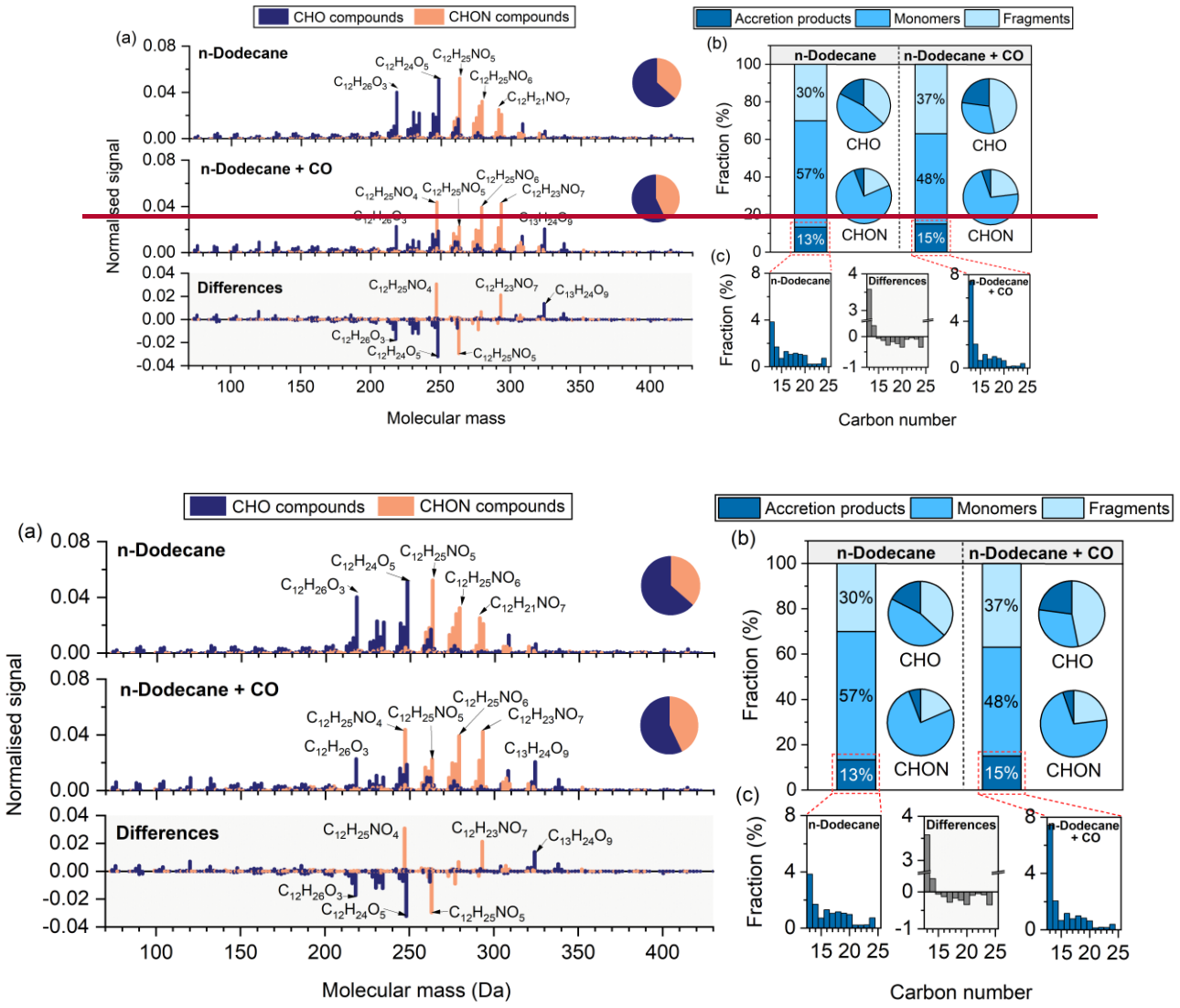

Figure ~~34~~: (a) High-resolution mass spectra of particle-phase compounds ~~identified~~measured by FIGAERO-CIMS in n-dodecane experiments conducted with and without CO, ~~along with their differences~~and the corresponding difference spectra (with CO minus without CO). Prominent peaks are labelled with their corresponding molecular formulas. All signal intensities are normalised to 1. Pie charts display the proportions of CHO and CHON ~~compounds~~groups. (b) Fractions of n-dodecane-derived fragments~~,~~ (C < 12), monomers~~,~~ (C = 12), and accretion products (C > 12) in the absence and presence of CO. Bar charts represent their relative contributions to the total signal, while pie charts show their ~~relative contributions~~ distribution within the CHO and CHON ~~compounds~~groups. (c) Carbon number

distributions of accretion products in the absence (left) and presence (right) of CO. The middle panel shows the differences between ~~them~~the two conditions (with CO minus without CO).

Compared to α-pinene, ~~the~~ particle-phase products derived from n-dodecane ~~had~~exhibited generally higher molecular mass distributions, ~~mainly~~primarily within the range of 210 ~~to~~ 310 Da (Fig. ~~3a). CHON compounds accounted for 37 % and 43 % of the total signal in the absence and presence of CO, respectively.~~4a). In the absence of CO, the most abundant ~~compounds~~species were $C_{12}H_{25}NO_5$, $C_{12}H_{24}O_5$, and $C_{12}H_{26}O_3$, whereas in the presence of CO, $C_{12}H_{25}NO_4$, $C_{12}H_{23}NO_7$, and $C_{12}H_{25}NO_3$ dominated. CHON compounds accounted for 37 % and 43 % of the total signal in the absence and presence of CO, respectively.

In the n-dodecane systems, compounds containing 12 carbon atoms were classified as monomers, those with fewer than 12 as fragments, and those with more than 12 as accretion products (Fig. ~~3b~~4b). Monomers dominated under both conditions, accounting for 57 % of the total signal in the absence of CO and 48 % in its presence. ~~Differences in carbon number distribution between~~Within the ~~two systems were primarily observed in the monomer~~ CHON group ~~(Fig. S10), with~~, monomers accounted for more than 70 %. The presence of CO ~~leading~~led to a lower proportion of C_{12} CHO compounds (e.g., $C_{12}H_{24}O_5$ and $C_{12}H_{26}O_3$) and a higher proportion of C_{12} CHON compounds (e.g., $C_{12}H_{25}NO_4$ and $C_{12}H_{23}NO_7$) ~~compared the experiment without CO (Fig. 3a). A~~(Fig. 4a). However, a few exceptions were observed. For example, ~~an increased contribution from~~ a series of highly oxygenated C_{13} CHO compounds, such as $C_{13}H_{24}O_9$ and $C_{13}H_{22}O_{10}$, ~~was detected~~accounted for a higher fraction in the presence of CO~~. In contrast,~~, whereas $C_{12}H_{25}NO_5$ ~~showed~~accounted for a higher ~~abundance~~fraction in the absence of CO. Fragments accounted for 30 % and 37 % in the absence and presence of CO, respectively. While the overall ~~contribution~~fraction of accretion products was comparable ~~between two systems~~under both conditions, the presence of CO ~~led to a~~ reduced the fraction of C_{16}–C_{24} accretion products ~~containing 16 – 24 carbon atoms compared to experiments without CO~~ (Fig. ~~3c~~4c).

~~The hydrogen atom number distribution of n-dodecane-derived CHO compounds displayed two peaks at 12 and 24 hydrogen atoms, likely corresponding to fragments and monomers products, respectively (Fig. S11). In the presence of CO, the relative abundance of CHO compounds containing 22, 24, and 26 hydrogen atoms were lower than those observed in the absence of CO. For the identified CHON species, compounds containing 25 hydrogen atoms were the most abundant. The presence of CO led to a general increase in the relative abundances of CHON compounds across the hydrogen atom numbers observed in this study.~~

The major RO_2 radicals derived from n-dodecane react via the R1 and R2 pathways to form the $C_{12}H_{24}O_n$ and $C_{12}H_{26}O_n$ families. As shown in Fig. 3, in the absence of CO these species accounted for 12.6 % and 10.4 % of the CHO group, respectively, and decreased to 5.6 % and 6.1 % in its presence.

3.3 Mixture

3.3.1 SOA particle mass ~~formation and~~ yields

During the first hour of the reaction, O_3 concentrations were comparable ~~between~~in the ~~two systems~~ absence and presence of

CO (Fig. 1a). Thereafter, ~~the CO present system exhibited higher~~ O_3 levels ~~than~~became higher in the presence of CO~~ absent system~~. In both cases, O_3 concentrations peaked during the final hour~~ of the reaction~~, reaching 81.1 ppb without CO and 101.6 ppb with CO.

The initial precursor/NO_x ratio was approximately 0.8 ~~± 0.2~~ (Table 1). NO_x concentrations declined steadily ~~under both conditions~~ throughout the reaction under both conditions (Fig. ~~S4~~S5). In the mixture, the presence of CO led to ~~slower~~lower decay rates for both α-pinene and n-dodecane compared to the experiment without CO (Fig. ~~1d~~1b). Nevertheless, α-pinene was fully consumed within three hours in both cases. By the end of the experiment, 25 % of the initial n-dodecane remained unreacted ~~in the absence of~~without CO, whereas 51 % remained ~~when~~with CO~~ was present~~.

In the absence of CO, the final SOA particle mass concentration reached 63.9 μg m^{-3}~~ of SOA particles were produced~~, corresponding to a mass yield of 0.11 (~~exp~~Exp. 9). In the presence of CO, it reached 58.8 μg m^{-3}~~ of SOA particles were formed~~, with a yield of 0.16.

3.3.2 SOA particle chemical composition

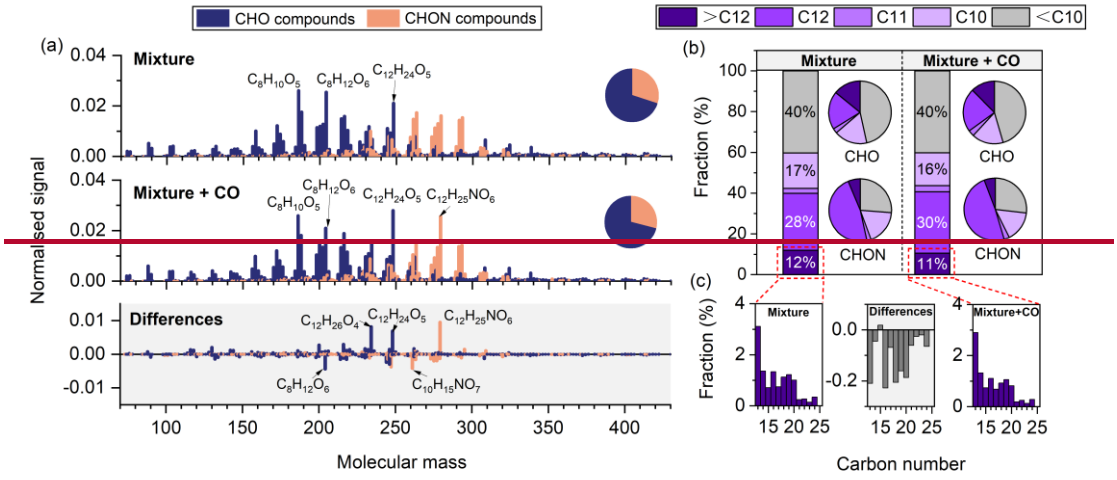

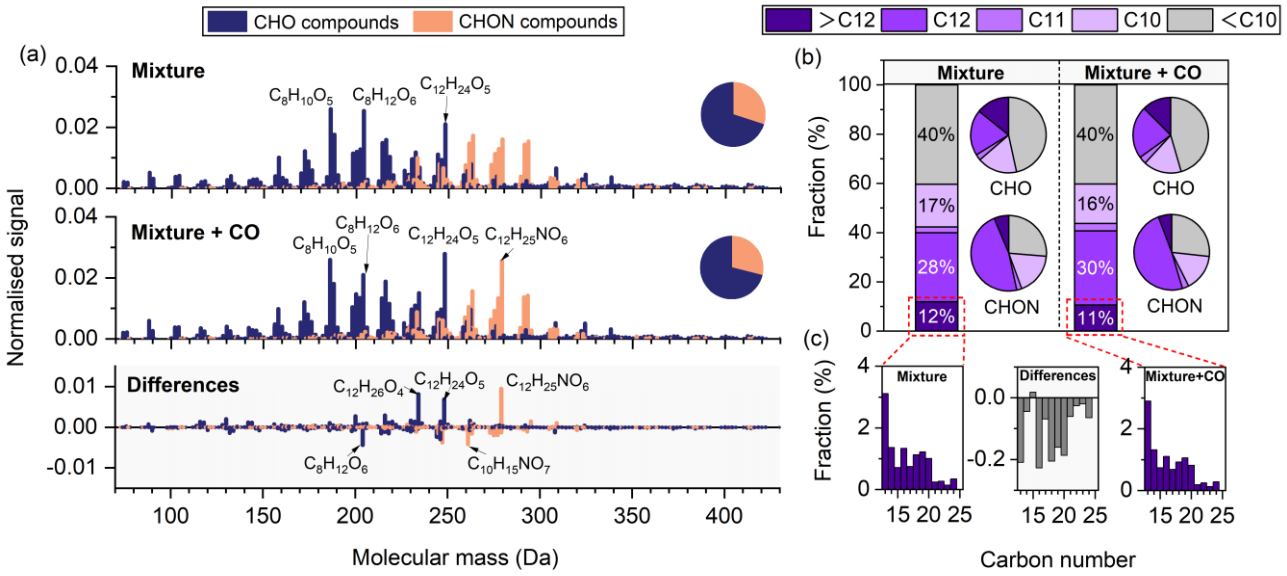

Figure 45: (a) High-resolution mass spectra of particle-phase compounds ~~identified~~measured by FIGAERO-CIMS in mixture experiments conducted with and without CO, ~~along with their differences~~and the corresponding difference spectra (with CO minus without CO). Prominent peaks are labelled with their corresponding molecular formulas. All signal intensities are normalised to 1. Pie charts display the proportions of CHO and CHON ~~compounds~~groups. (b) Fractions of particle-phase products with different carbon numbers in the absence and presence of CO. Bar charts represent their relative contributions to the total signal, while pie charts show their ~~relative contributions~~ distribution within the CHO and CHON ~~compounds~~groups. (c) Carbon number distributions of products with more than 12 carbon atoms in the absence (left) and presence (right) of CO. The middle panel shows the differences between ~~them~~the two conditions (with CO minus without CO).

Compared to single-precursor systems, the mixed-precursor system exhibited a broader molecular mass distribution, ~~mainly~~primarily ranging from 150~~ to~~ 330 Da (Fig. ~~4a).~~5a). In the absence of CO, $C_8H_{10}O_5$, $C_8H_{12}O_6$, and $C_{12}H_{24}O_5$ showed the highest signal intensities, whereas in the presence of CO, $C_{12}H_{24}O_5$, $C_8H_{10}NO_5$, and $C_{12}H_{25}NO_6$ were most abundant. CHON compounds accounted for 30 % and 29 % of the total signal in the absence and presence of CO, respectively. ~~In the absence of CO, $C_8H_{10}O_5$, $C_8H_{12}O_6$, and $C_{12}H_{24}O_5$ had the highest signal intensities, whereas in the presence of CO, the most abundant compounds were $C_{12}H_{24}O_5$, $C_8H_{10}NO_5$, and $C_{12}H_{25}NO_6$.~~

In the mixture, ~~the complexity of interactions made it difficult to clearly distinguish monomers, fragments, and accretion products. Nevertheless,~~ compounds with fewer than 10 carbon atoms were ~~reasonably~~ classified as fragments, while those containing more than 12 carbon atoms were considered accretion products. ~~As shown in Fig. S10, the effect of CO on the carbon distribution in the mixture was generally less pronounced than in the single-precursor systems. While the relative abundances of C10, C12, and accretion products (C>12) were similar~~Fragments dominated under both conditions ~~(Fig 4b), small shifts~~and accounted for 40 % of the total signal in ~~composition were evident~~each case. Accretion products accounted for

12 % and 11 % in the absence and presence of CO, ~~displaying features distinct from those in the single precursor systems. Specifically, CO led to (i) a slightly lower fraction of accretion products containing 13 to 24 carbon atoms (excluding~~respectively. Except for C_{15}~~) (Fig. 4c), (ii) an increased~~ species, the fractions of C_{13}–C_{24} products decreased slightly in the presence of CO. In addition, the presence of CO resulted in an increased proportion of C_{12} CHO compounds (e.g., $C_{12}H_{26}O_4$ and $C_{12}H_{24}O_5$), and ~~(iii)~~ a reduced proportion of C_{10} CHON compounds (e.g., $C_{10}H_{15}NO_7$) (Fig. ~~4a).~~

~~As shown in Fig. S11, the hydrogen atom~~ 5a). Overall, changes in carbon number distribution ~~of mixture derived CHO compounds showed two peaks at 14 and 24 hydrogen atoms, with the peak at 14 being the most abundant. In the presence of CO, the relative abundances of CHO compounds with 12 and 14 hydrogen atoms decreased, while those with 16, 24, and 26 hydrogen atoms increased. Among the identified CHON species, the presence of CO resulted in an increased fraction of 25-hydrogen compounds and a decreased fraction of 15 hydrogen compounds.~~were less pronounced in the mixed-precursor system than in the single-precursor systems (Fig. S11).

The bottom panel of Fig. 3 shows the relative contributions of $C_{10}H_{14}O_n$, $C_{10}H_{16}O_n$, $C_{10}H_{18}O_n$, $C_{12}H_{24}O_n$, and $C_{12}H_{26}O_n$ to the CHO products in the mixture. In the presence of CO, the fractions of $C_{10}H_{14}O_n$ and $C_{10}H_{18}O_n$ decreased from 6.9 % and 1.2 % to 5.5 % and 0.8 %, respectively, whereas those of $C_{10}H_{16}O_n$, $C_{12}H_{24}O_n$, and $C_{12}H_{26}O_n$ increased from 7.6 %, 5.0 %, and 3.1 % to 10.4 %, 6.6 %, and 4.7 %, respectively.

4 Discussion

4.1 Photochemistry

The photochemical reactions in this study involved the simultaneous presence of NO_x and CO, multiple oxidants (OH and O_3), ~~as well as~~and multiple precursor species. The interactions among these factors substantially ~~increased~~increase the complexity of the system, making it challenging to establish comparable experimental conditions ~~that allow for a comparison~~ across different precursor systems. ~~To address~~In this study, two key approaches were adopted: (i) ensuring initial iso-reactivity towards OH radicals, and (ii) ~~maintaining~~setting comparable initial precursor/NO_x ratios across systems. Additionally, an oxidant closure approach was employed to characterise the photochemical conditions. As OH radicals could not be directly measured ~~directly~~ in this study, their concentrations were estimated from the temporal evolution of O_3 and the consumption of precursors, or alternatively~~,~~ from the depletion of CO~~.~~ (see details in the Supplementary Information). This approach enabled a quantitative evaluation of the relative contributions of different oxidants to precursor oxidation.

~~This study was designed for OH radicals to serve as the predominant photochemical loss of precursors.~~ Under idealised iso-reactivity conditions, all systems ~~exhibited~~would exhibit comparable initial OH reactivity, and in the mixture ~~experiments,~~ each precursor molecule would initially ~~had~~have an equal probability of reacting with OH. ~~However, as the reaction progressed~~In practice, however, O_3 ~~gradually accumulated and became increasingly important for the~~also contributed to precursor oxidation ~~of O_3-reacting precursors, resulting in the coexistence of two oxidants in the system. Due to~~, and the differing reactivities of individual precursors towards O_3~~, their decay rates varied accordingly (Fig. 1c-d). In the experiments without CO,~~ can modify the precursor decay and secondary oxidant formation, thereby influencing the reactivity. n-Dodecane was oxidised exclusively by OH radicals. For α-pinene, although OH remained the dominant photochemical sink in this study, the contribution of O_3 to its decay was not negligible. As shown in Fig. S12, the relative contributions of these oxidants evolved over time, with the role of O_3 generally becoming more important as the reaction proceeded. In the α-pinene single-precursor system, on average approximately ~~70~~80 % of α-pinene decay was ~~attributed~~attributable to OH oxidation, while the remaining ~~30 % was driven by ozonolysis (Fig. S12). OH dominated during the early stage of the reaction, contributing over 90 % to α-pinene consumption. However, as the reaction proceeded, the contribution of O_3 became increasingly significant, accounting for over 40 % in the mixture. In contrast, n-dodecane does not react with O_3 and was oxidised exclusively via OH radicals. Thus, although OH remained the dominant oxidant for α-pinene oxidation, the contribution from ozonolysis was still non-negligible.~~ ~20 % was driven by ozonolysis. By comparison, the contribution of ozonolysis was slightly higher in the mixed-precursor system. Thus, fully comparable reactivity across different systems was difficult to maintain throughout the reaction when multiple oxidants were present. This reflects an inherent limitation of defining iso-reactivity with respect to a single oxidant in multi-oxidant systems.

The precursor/NO_x ratio is important for determining the chemical regime of O_3 and SOA formation (Chen et al., 2022)~~Owing to the chemical coupling among O_3, NO_x, and RO_x (= OH + RO_2 + HO_2), NO_x plays a critical role in determining both the oxidation conditions and the fate of RO_2 radicals, thereby influencing the yields and chemical composition of SOA particles. In this study, NO_x served as the source of OH via O_3 photolysis. The initial precursor/NO_x ratios were maintained at similar~~

~~levels among different systems, which aimed to minimise systematic discrepancies arising from variations in reaction pathways and thus enabled a more reliable assessment of the effects of CO. Estimated OH levels were largely comparable across systems in the absence of CO (Fig. S5). During the first hour of reaction, O_3 concentrations were also similar, but subsequently both their levels and temporal profiles diverged, leading to differences in overall oxidant levels.~~. However, when multiple precursors are involved, maintaining similar initial precursor/NO_x ratios may not be sufficient to establish comparable chemical regimes across systems. In this study, the temporal profiles of O_3 and NO_x differed substantially between the single- and mixed-precursor systems (Figs. 1a and S5). In the α-pinene system, O_3 concentrations peaked after approximately two hours of reaction and subsequently declined, while NO_x levels stabilised ~~(Fig. 1a and S4). At~~. By this point, over 80 % of α-pinene had been consumed, and the SOA particle formation rate ~~also~~ began to decline (~~Fig~~Figs. 1b~~–~~c). These trends may indicate a ~~diminished rate of~~ reduction in RO_2 + NO reactions~~. The reduced RO_2 + NO reactivity slowed the depletion of NO~~, which ~~in turn enhanced the titration of~~would slow the conversion of NO to NO_2 and thereby limit photochemical O_3 ~~and led to a net O_3 loss~~production. In contrast, in the n-dodecane and mixture systems, over 50 % of n-dodecane was still unreacted after two hours ~~of reaction~~, and the SOA particle formation rate continued to increase (~~Fig~~Figs. 1b ~~d~~ –c), indicating that ~~the~~ RO_2 + NO ~~pathway~~reactions remained active. This sustained reactivity enabled continuous conversion of NO ~~consumption, which in turn limited O_3 titration~~to NO_2 and ~~let to a net accumulation of O_3~~enhanced photochemical O_3 production.

These results raise an important consideration for studies involving multiple precursors and oxidants. Even when ~~the~~ initial OH reactivity and precursor/NO_x ratios are controlled, ~~differences in precursor reactivities and the close coupling between secondary oxidant formation and precursor oxidation make it challenging to maintain~~achieving fully comparable ~~chemical regimes~~experimental conditions across such systems~~. As~~ remains challenging. Given that the coexistence of multiple precursors and oxidants is a common feature of the ambient atmosphere, future ~~chamber~~laboratory studies should ~~investigate~~explore a broader range of precursor/NO_x ratios and systematically assess the effects of varying oxidants to improve our understanding of SOA formation under atmospherically relevant ~~oxidative~~ conditions.

The addition of CO further perturbed the photochemical processes, altering both oxidant levels and precursor decay rates. ~~Previous studies have demonstrated that CO can suppress SOA particle formation through two main factors: (i) competition with precursors for OH, which is referred to as oxidant (OH) scavenging, and (ii) an elevated HO_2/RO_2 ratio, which favoured RO_2 + HO_2 termination pathways rather than RO_2 + RO_2 reactions, thereby reducing the formation of accretion products, known as the product scavenging~~CO can consume OH radicals, preventing their reaction with SOA precursors (McFiggans et al., 2019). ~~At~~Based on the estimated OH concentrations, evidence for this oxidant scavenging effect was observed. During the initial stage of the reaction, CO reduced the OH concentrations by approximately 50 % to around 1.5×10^6 molecules cm^{-3} (Fig. ~~S5). However, as the reaction progressed, OH levels gradually recovered and eventually reached values comparable to those observed in the absence of CO.~~S6). However, OH levels gradually recovered as the reaction progressed and eventually reached values comparable to those observed in the absence of CO (except for n-dodecane system). In the presence of CO, the reaction of CO with OH led to enhanced HO_2 formation. Subsequent HO_2 + NO reactions regenerated OH, thereby increasing radical propagation efficiency. In contrast, in the absence of CO, although O_3 photolysis provided a primary source of OH, OH regeneration in the n-dodecane system was likely less efficient, consistent with the decline in OH concentrations. In both the

α-pinene and mixture systems, however, OH concentrations continued to increase even without CO, indicating the presence of additional OH regeneration processes, such as OH formation during α-pinene ozonolysis. In addition to its impact on OH concentrations, the presence of CO also modified O_3 levels. In the presence of CO, both the α-pinene and mixture systems exhibited higher peak O_3 concentrations, whereas ~~in~~ the n-dodecane system ~~O_3~~ showed generally lower O_3 levels. Variations in oxidant concentrations ~~were generally lower. As shown~~contributed to changes in ~~Fig 1c-d, CO influenced the~~SOA precursor decay rates ~~of~~ (Fig. 1b). In the absence of CO, α-pinene ~~and n-dodecane to different extents. In the α-pinene system, although the α-pinene decay rate~~ was ~~reduced in the~~ almost completely consumed within 3 h. In the presence of CO, ~~the total consumption remained unchanged, and the relative contributions of OH and O_3 showed little variation (Fig. S12). These results suggest that the effect of OH scavenging on~~its decay was initially suppressed; however, after approximately 2 h the decay ~~of α-pinene was limited. For n-dodecane, OH scavenging had~~ rate increased, likely due to secondary OH production and elevated O_3 concentrations. Such that α-pinene was nevertheless nearly fully consumed within 3 h. As a ~~pronounced effect on its decay, with~~result, CO did not significantly ~~reducing both the~~ affect the overall extent of α-pinene consumption. In contrast, for n-dodecane, the presence of CO not only slowed the oxidation rate but also reduced the overall extent of consumption ~~rate and overall consumption (Fig. 1c-d).~~ , leaving a substantial fraction unreacted by the end of the experiment.

4.2 Effect of CO on SOA particle chemical composition

4.2.1 Single-precursor systems

The presence of CO led to several consistent changes in the chemical composition of SOA particles in both the α-pinene and n-dodecane systems, including an increased relative contribution of the CHON group and fragment species and a reduced fraction of C_{16}–C_{24} accretion products (Figs. 2 and 4). In addition, the relative contributions of representative RO_2 + RO_2 termination products ($C_{10}H_{14}O_n$ and $C_{12}H_{24}O_n$) within the CHO group decreased (Fig. 3). These observations provide evidence for a similar shift in RO_2 fate in the presence of CO in both systems. However, owing to the limitations of I^--CIMS measurements, the absolute contributions in individual reaction pathways cannot be fully constrained. The following discussion is therefore based partly on relative changes.

Organic nitrate concentrations were estimated from AMS measurements using the method described by Kiendler-Scharr et al. (2016). The results show that, in the single-precursor systems, the presence of CO led to a pronounced reduction in organic nitrate concentrations (Fig. S13). This reduction can be attributed to two main factors. First, CO competes with SOA precursors for available OH (Figs. 1b and S6). Second, CO enhances HO_2 formation, increasing the importance of the RO_2 + HO_2 pathway and thereby altering RO_2 reaction branching. In addition, lower NO concentrations were observed in the presence of CO (Fig. S5), consistent with enhanced conversion of NO to NO_2 via the HO_2 + NO reaction. The increase in HO_2 and decrease in NO reduced the likelihood of RO_2 reacting with NO. Despite this absolute reduction, FIGAERO-CIMS results showed that the relative contributions of the CHON group and fragment products increased in the presence of CO (Figs. 2 and 4). CHON products are primarily formed through the RO_2 + NO → $RONO_2$ pathway, and fragment species originate from the fragmentation of RO radicals (Atkinson, 2000; Ziemann and Atkinson, 2012). Owing to the rapid reaction of RO_2 with NO

and the high branching towards RO formation, reactions of RO_2 with NO represent an important source of RO radicals under NO_x conditions (Orlando et al., 2003; Ziemann and Atkinson, 2012). These observations therefore indicate that, in the presence of CO, the contribution of RO_2 + NO reactions decreased, but to a lesser extent than competing RO_2 termination pathways.

AMS measurements showed a decrease in SOA particle mass concentrations in the presence of CO (Fig. 1c). In addition to OH scavenging, another important factor is that CO enhances competition between RO_2 + RO_2 and RO_2 + HO_2 reactions, thereby reducing the formation of accretion products (Baker et al., 2024; McFiggans et al., 2019; Peräkylä et al., 2023). Despite this reduction, CO did not significantly alter the overall fraction of accretion products. However, the relative contribution of C_{16}–C_{24} species decreased (Figs. 2c and 4c), accompanied by an increase in C_{11}–C_{15} species in the α-pinene system and C_{13}–C_{14} species in the n-dodecane system. Accretion products with lower carbon numbers are expected to form via pathways that involve fragmentation of RO radicals (Kang et al., 2025), and their increased relative contribution is consistent with the elevated fraction of fragment products discussed above. In contrast, longer-chain accretion products are more likely to originate from RO_2 + RO_2 reactions involving non-fragmented C_{10}/C_{12} RO_2 radicals, including reactions between non-fragmented RO_2 radicals and fragmented RO_2 radicals (< C_{10}), or between two non-fragmented RO_2 radicals, yielding C_{20} and C_{24} accretion products in the α-pinene and n-dodecane systems, respectively. Combined with the reduced fractions of $C_{10}H_{14}O_n$ and $C_{12}H_{24}O_n$ families (Fig. 3), these observations indicate that CO preferentially suppressed RO_2 + RO_2 chemistry, particularly pathways forming longer-chain accretion products.

Overall, in the single-precursor systems, CO reduced the contributions of both RO_2 + RO_2 and RO_2 + NO reactions. However, reactions of RO_2 with NO decreased to a lesser extent than competing RO_2 termination pathways, and the reduction in RO_2 + RO_2 termination was more pronounced for longer-chain accretion products than for shorter-chain ones.

4.2.2 Mixed-precursor system

Compared with the single-precursor systems, the influence of CO on SOA chemical composition differed in the mixed-precursor system. Specifically, (i) the presence of CO did not significantly alter the relative contributions of the CHON group and fragment species (Figs. 5a–b); (ii) the fractions of C_{13}–C_{24} accretion products (excluding C_{15}) slightly decreased (Fig. 5c); and (iii) within the CHO group, the fraction of the $C_{10}H_{14}O_n$ family decreased, whereas that of the $C_{12}H_{24}O_n$ family increased (Fig. 3).

In the mixed-precursor system, organic nitrate concentrations exhibited little variation in the presence of CO (Fig. S13), consistent with the largely unchanged relative contribution of the CHON group and fragment species. This suggests that the contribution of RO_2 + NO reactions was not substantially reduced under CO conditions.

SOA particle mass concentrations and the fraction of accretion products both decreased slightly in the presence of CO (Figs. 1c and 5), suggesting a slight reduction in the contribution of RO_2 + RO_2 termination.

Moreover, CO led to a lower fraction of the $C_{10}H_{14}O_n$ family in the mixture, consistent with the trend observed in the α-pinene

single-precursor system. In contrast to the n-dodecane single-precursor system, however, the relative contribution of the $C_{12}H_{24}O_n$ family increased in the presence of CO in the mixture. Together with the increase in the fraction of C_{12} species and decrease in that of C_{10} species (Fig. S11), these observations may indicate that CO affected RO_2 + RO_2 termination involving α-pinene-derived RO_2 more strongly than that involving n-dodecane-derived RO_2.

Overall, in the mixed-precursor system, the influence of CO on RO_2 termination pathways was less pronounced than in the single-precursor systems and may have affected n-dodecane- and α-pinene-derived RO_2 to different extents.

Although the underlying mechanism cannot be fully resolved in this study, the observed changes in product distributions provide important evidence for shifts in RO_2 reaction pathways in the mixed-precursor system under different conditions. As α-pinene and n-dodecane were used as representative precursors, these findings may be specific to the present system. Future chamber studies covering a broader range of precursor combinations are therefore needed to assess the generality of the observed behaviour.

4.3 Effect of CO on SOA particle mass yields

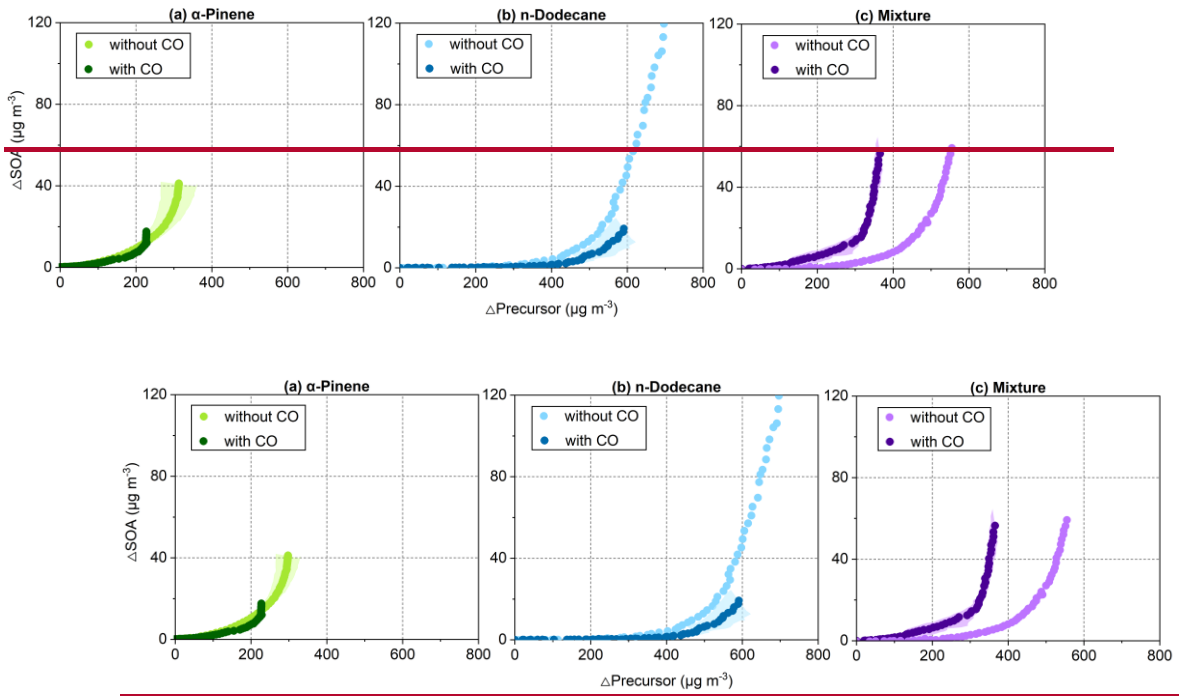

Figure ~~5~~6: Growth curves of SOA particles ~~formed from~~for (a) α-pinene, (b) n-dodecane, and (c) mixture experiments, defined as the ratio of ~~the~~SOA particle mass ~~concentrations of formed SOA particles~~concentration to ~~the reacted~~consumed precursor mass ~~of precursors~~. Shaded areas represent the ~~envelope from repeated~~range between replicate experiments.

~~The influence of CO on SOA particle mass yields differed significantly between the single-precursor and mixture systems. In the single-precursor systems, CO consistently suppressed the yields, with the effect being more pronounced for n-dodecane than for α-pinene. In the presence of CO, SOA particle mass concentration and yield decreased by 83 % and 79 % for n-dodecane, and by 57 % and 43 % for α-pinene, respectively. One possible factor contributing to this difference is that OH scavenging effect was stronger in the n-dodecane than in the α-pinene system. By contrast, in the mixture, even though OH scavenging was evident, the presence of CO led to only an 8 % decrease in SOA particle mass concentration, whereas the final mass yield showed an increase. To better understand this observation, it may be necessary to distinguish the respective contributions of OH scavenging and product scavenging to the overall effects of CO on yields. Future relevant studies should therefore consider compensating for OH loss to clarify the individual roles of these two scavenging processes .~~

~~Fig. 5~~Figure 6 presents the SOA particle growth curves for each system. The slope of the curve represents the incremental SOA particle mass yield at a given stage of precursor consumption, while the final position of the curve reflects the overall yield achieved by the end of the experiment. The induction period is defined as the amount of SOA precursor consumed before SOA particle formation begins (Zhou et al., 2019). Compared with the α-pinene~~,~~ system, the n-dodecane ~~systems had~~system exhibited a longer induction period, ~~with the mixture falling~~while that of the mixed-precursor system lay in between. In the presence of CO, the induction period was extended in the n-dodecane system but remained largely unchanged in the α-pinene system. Notably, the induction period in the mixture system was shortened in the presence of CO. ~~This phenomenon suggests~~These behaviours suggest a distinct influence of CO on the SOA ~~formation pathways in the mixed-precursor system compared with the single-precursor~~particle mass yields across different systems~~, as will be discussed in the following section. .~~

In the single-precursor systems, CO substantially reduced SOA formation, with a stronger effect for n-dodecane than for α-pinene. In the presence of CO, SOA particle mass concentrations and overall yields decreased by 83 % and 79 %, respectively, for n-dodecane, and by 57 % and 43 % for α-pinene. In contrast, the mixed-precursor system exhibited only an 8 % decrease in SOA mass concentration, and the overall yield increased slightly.

Chemical composition analysis indicates that, in the single-precursor systems, the contributions of accretion products derived from RO_2 + RO_2 termination, particularly those with longer carbon chains, decreased in the presence of CO. These accretion products are expected to exhibit extremely low volatility and contribute efficiently to SOA formation (Peräkylä et al., 2023). At the same time, although the absolute concentration of organic nitrates decreased, the fractions of CHON and fragment products increased in the presence of CO. This suggests that RO_2 + NO reactions were also reduced, but less markedly than the competing RO_2 termination pathways. Products formed via RO_2 + NO reactions are generally expected to exhibit higher volatility than those formed through RO_2 + HO_2 and RO_2 + RO_2 termination (Presto et al., 2005; Zhao et al., 2018). All these changes are therefore expected to shift the product distribution towards more volatile species, consistent with the observed decrease in SOA particle mass yields.

Compared with the single-precursor systems, changes in RO_2 reaction pathways in the mixture appeared to exert a weaker influence on the formation of lower-volatility products. Consequently, SOA particle mass concentrations and yields behaved

differently in the mixed-precursor system.

Competition between CO and SOA precursors for available OH was also a factor influencing the yields (McFiggans et al., 2019). However, the impact of differences in OH concentrations on SOA particle mass yields and chemical composition cannot be fully assessed in this study. Future work may need to re-adjust OH concentrations so that the systems can be maintained at comparable oxidation stages, thereby enabling more direct comparisons (Baker et al., 2024; McFiggans et al., 2019)~~**4.3 Effect of CO on SOA particle chemical composition**~~

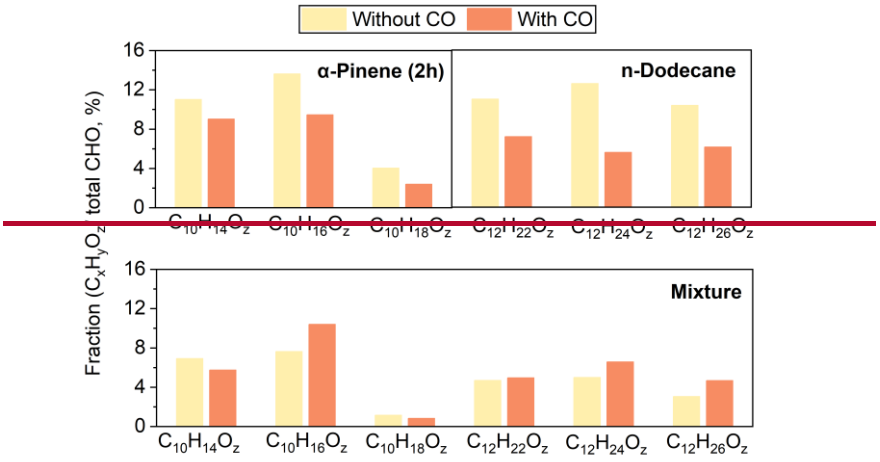

~~**Figure 6: Relative contributions of $C_{10}H_{14}O_z$, $C_{10}H_{16}O_z$, $C_{10}H_{18}O_z$, $C_{12}H_{22}O_z$, $C_{12}H_{24}O_z$, and $C_{12}H_{26}O_z$ to the total CHO compounds in the α-pinene, n-dodecane, and mixture systems in the absence and presence of CO.**~~

~~**4.3.1 Single-precursor systems**~~

~~The presence of CO led to several consistent changes in the chemical composition of SOA particles in both the α-pinene and n-dodecane systems, including an increased contribution of CHON compounds, a reduced fraction of C_{16} to C_{24} accretion products, and shifts in the distribution of hydrogen atom numbers. These observations provide evidence for a similar alteration in RO_2 fate in the presence of CO for both systems.~~

~~CHON compounds constituted a significant fraction of the SOA particles, indicating that reactions with NO were also an important RO_2 termination pathway in our experiments. In the presence of CO, the increase in total CHON fractions in both α-pinene and n-dodecane systems was mainly attributed to enhanced contributions from specific C_{10} and C_{12} CHON~~

compounds, respectively (Fig. S10). These findings suggest that the suppression of RO_2 + RO_2 termination pathways induced by CO may have increased the relative importance of monomer-derived RO_2 + NO reactions.

The presence of CO did not significantly alter the overall contribution of accretion products to the SOA particles in the single-precursor systems. However, the contribution of those containing 16 to 24 carbon atoms decreased in both systems (Fig. 2c and 3c). Correspondingly, in the α pinene system, the relative abundance of accretion products with 11 to 15 carbon atoms increased, while in the n-dodecane system, those with 13 to 14 carbon atoms became more abundant. Accretion products are typically formed via the chemical bonding of two RO_2 radicals . Compounds with fewer carbon atoms are likely derived from reactions involving fragment-derived RO_2 radicals, whereas those with higher carbon numbers are more likely formed through reactions between monomer-derived RO_2 radicals and fragment-derived RO_2 radicals, or between two monomer-derived RO_2 radicals . An elevated HO_2/RO_2 ratio can suppress RO_2 + RO_2 pathway, thereby altering the product distribution. Previous studies have quantitatively assessed the effect of CO on the chemical composition of SOA from α pinene, reporting a twofold reduction in C_{17} to C_{20} HOM dimers . After compensating for the OH consumption by CO, α pinene-derived HOM accretion products were reduced by approximately 60% under CO present conditions . In this study, quantitative assessment of accretion product concentrations was not possible due to instrumental limitations. Nevertheless, based on the changes in the relative contributions of accretion products and the SOA particle mass concentration, it can be inferred that the suppression effect of CO on RO_2 + RO_2 reactions was more pronounced for monomer-derived RO_2 radicals than for fragment-derived ones.

The shifts in hydrogen atom distributions further supported the above interpretation of altered RO_2 termination pathways under CO present conditions. Fig. S11 presents the distribution of hydrogen atom numbers across different systems. Similar patterns were observed in both the α pinene and n-dodecane systems. In the α pinene system, the presence of CO led to a decrease in the relative abundance of CHO compounds containing 14, 16, and 18 hydrogen atoms. Specifically, the relative contributions of $C_{10}H_{14}O_z$, $C_{10}H_{16}O_z$, and $C_{10}H_{18}O_z$ species to CHO compounds were reduced by 2.0 %, 4.2 %, and 1.6 %, respectively, in the presence of CO (Fig. 6). The main RO_2 radicals generated from α pinene photooxidation are $C_{10}H_{15}O_x$ and $C_{10}H_{17}O_x$. HO_2 termination of $C_{10}H_{15}O_x$ radicals forms multifunctional hydroperoxides ($C_{10}H_{16}O_z$), whereas RO_2 termination produce $C_{10}H_{14}O_z$ carbonyls and $C_{10}H_{16}O_z$ alcohols. Similarly, HO_2 termination of $C_{10}H_{17}O_x$ radicals form $C_{10}H_{18}O_z$ hydroperoxides, and RO_2 termination yield $C_{10}H_{16}O_z$ carbonyls and $C_{10}H_{18}O_z$ alcohols. Cross reactions between $C_{10}H_{15}O_x$ and $C_{10}H_{17}O_x$ radicals lead to the formation of $C_{10}H_{14}O_z$ carbonyls and $C_{10}H_{18}O_z$ alcohols, and/or $C_{10}H_{16}O_z$ carbonyls and alcohols. Therefore, while $C_{10}H_{16}O_z$ and $C_{10}H_{18}O_z$ species can be produced through multiple termination pathways, the formation of $C_{10}H_{14}O_z$ occurs exclusively via RO_2 + RO_2 reactions. For n-dodecane, the presence of CO led to a decrease in the relative abundance of CHO compounds containing 22, 24, and 26 hydrogen atoms. Specifically, the relative contributions of $C_{12}H_{22}O_z$, $C_{12}H_{24}O_z$, and $C_{12}H_{26}O_z$ species decreased by 3.8 %, 7.0 %, and 4.2 %, respectively, in the presence of CO (Fig. 6). The discussion here focuses primarily on the $C_{12}H_{24}O_z$ and $C_{12}H_{26}O_z$ families. The main RO_2 radicals generated from n-dodecane photooxidation is $C_{12}H_{25}O_x$. HO_2 termination yields $C_{12}H_{26}O_z$ hydroperoxides, while RO_2 termination produce $C_{12}H_{24}O_z$ carbonyls and $C_{12}H_{26}O_z$ alcohols. The $C_{12}H_{24}O_z$ family is formed exclusively through RO_2 + RO_2 reactions. The reductions in the relative abundances of $C_{10}H_{14}O_z$ and $C_{12}H_{24}O_z$ in the α pinene and n-dodecane systems, respectively, thus provide further evidence that the presence of CO suppressed the RO_2 + RO_2 reaction pathway.

~~**4.3.2 Mixed-precursor system**~~

~~Compared with the single-precursor systems, the influence of CO on the chemical composition of SOA in the mixed-precursor system was different: (i) the addition of CO did not significantly alter the proportion of CHON compounds, indicating that the relative importance of the RO_2 + NO pathway remained largely unchanged; (ii) the relative contributions of C_{13} to C_{24} accretion products (excluding C_{15}) slightly decreased, indicating a moderate suppression of the RO_2 + RO_2 pathway; (iii) the changes in hydrogen atom distributions differed from those observed in the single-precursor systems, possibly implying a distinct influence on the RO_2 reaction pathways.~~

~~In the mixed-precursor system, RO_2 termination reactions were expected to be more complex than those in single-precursor systems. In addition to the pathways discussed above, cross-reactions between RO_2 radicals originating from different precursors may also occur. RO_2 + RO_2 reactions between $C_{10}H_{15}O_x$ and $C_{12}H_{25}O_x$ yield $C_{10}H_{14}O_z$ carbonyls and $C_{12}H_{26}O_z$ alcohols or $C_{12}H_{24}O_z$ carbonyls and $C_{10}H_{16}O_z$ alcohols. Similarly, reactions between $C_{10}H_{17}O_x$ and $C_{12}H_{25}O_x$ lead to the formation of $C_{10}H_{16}O_z$ carbonyls and $C_{12}H_{26}O_z$ alcohols, or $C_{12}H_{24}O_z$ carbonyls and $C_{10}H_{18}O_z$ alcohols. In the mixture, the presence of CO led to a decrease in the relative contributions of $C_{10}H_{14}O_z$ and $C_{10}H_{18}O_z$ families by 1.2 % and 0.3 %, respectively, while the relative contributions of $C_{10}H_{16}O_z$, $C_{12}H_{24}O_z$, and $C_{12}H_{26}O_z$ families increased by 2.8 %, 1.6 %, and 1.6 %, respectively (Fig. 6). Based on the carbon number distributions observed in the single-precursor systems, it was reasonably assumed that C_{10} compounds in the mixture primarily originated from α-pinene, while C_{12} compounds were mainly derived from n-dodecane. The decrease in the fraction of the $C_{10}H_{14}O_z$ family suggests that, in the presence of CO, the relative abundance of the RO_2 termination involving α-pinene derived RO_2 and/or cross-reactions between $C_{10}H_{15}O_x$ and $C_{12}H_{25}O_x$ became less pronounced in the mixture. In contrast, the relative abundance of $C_{12}H_{24}O_z$ family increased in the mixture in the presence of CO. Taken together with the observed increase in the contribution of C_{12} species and decrease in C_{10} species in the mixture (Fig. S10), this suggest that CO exerted a weaker suppression effect on cross-reactions involving n-dodecane derived RO_2 than on those involving α-pinene derived RO_2. However, due to the lack of quantitative measurements on individual accretion products, the extent of this effect remains unclear. Moreover, as α-pinene and n-dodecane were used as representative precursors, the findings may be specific to the present system. These uncertainties highlight the need for future chamber studies to investigate a broader range of precursor combinations to assess the generality of the observed behaviour.~~

~~5.~~

5 Conclusions and implications

We established a photochemical system in the MAC that incorporated both biogenic and anthropogenic ~~precursors, together with coexisting CO and NO_x. Compared to the chamber studies conducted under simplified conditions, this setup is more representative of polluted atmospheric environments, enabling a better characterisation of real-world SOA formation processes. Our findings show that, under altered reaction conditions, the changes in~~SOA precursors in the presence of CO and NO_x. The results show that the influence of CO on SOA particle mass yields and chemical composition differed markedly between single- and mixed-precursor systems.

In the single-precursor systems, the presence of CO led to a notable reduction in SOA particle mass yields, with a stronger effect for n-dodecane than for α-pinene. By contrast, no such suppression was observed in the mixture. Chemical composition analysis indicated that, in the single-precursor systems, CO reduced the contributions of both RO_2 + RO_2 and RO_2 + NO reactions. In the mixed-precursor system, however, RO_2 + NO reactions showed no evident reduction, while the decrease in RO_2 + RO_2 termination was comparatively small. In addition, CO affected the two precursors to different extents in the mixture.

Although biogenic precursors contribute more substantially to SOA formation on a global scale, anthropogenic precursors can play a significant role in urban and suburban environments (Srivastava et al., 2022; Stone et al., 2010; Volkamer et al., 2006). Such regions are often characterised by elevated levels of ~~other~~co-emitted pollutants ~~with strong anthropogenic sources~~, such as CO and NO_x, which can ~~alter~~modify oxidant budgets and shift radical reaction pathways. Consequently, model parameterisations derived under single-precursor or idealised conditions may misrepresent SOA formation in non-~~clean~~pristine environments. Future laboratory studies should ~~simulate~~better capture the chemical complexity of the real atmosphere ~~by incorporating representative precursor mixture~~to improve the accuracy and ~~common trace gases, thereby providing a more reliable basis for the development~~applicability of ~~accurate~~ SOA model parameterisations.

However, establishing experimental conditions that account for atmospheric chemical complexity while remaining comparable across different systems remains challenging. The nonlinear interactions among multiple precursors, inorganic trace gases, and oxidants substantially increase the complexity of the system. In this study, even when the initial ~~experimental conditions were designed to maintain comparable~~ OH reactivity and precursor/NO_x ratios ~~and iso-reactivity towards OH across systems. However, results showed that variations in oxidant levels still led to differences in precursor decay rates and potentially the SOA formation.~~were controlled, fully comparable conditions across such systems could not be achieved. This highlights the need for ~~carefully defining comparable reaction conditions across parallel experiments involving complex photochemical systems where multiple precursors and oxidants coexist. Future~~future work ~~should~~to systematically investigate SOA formation under controlled variations in oxidant levels and precursor/NO_x ratios to ~~improve~~enhance the reliability and comparability of ~~experimental~~ results.

~~6 Conclusions~~

~~This study investigated the impact of CO on SOA particle mass yields and chemical composition from a biogenic VOC (α-pinene), an anthropogenic IVOC (n-dodecane), and their mixture in the presence of NO_x. The results indicate that the effects differed between the single- and mixed-precursor systems.~~

~~In the single-precursor systems, the presence of CO led to a notable reduction in SOA particle mass yields, with the suppression being more pronounced for n-dodecane than for α-pinene. By contrast, no such suppression was observed in the mixture.~~

~~Chemical composition analysis revealed consistent trends in the single-precursor systems, indicating similar shifts in RO_2~~

~~termination pathways. In both α-pinene and n-dodecane single precursor systems, the presence of CO increased the relative abundance of CHON species and decreased the fraction of C_{16} to C_{24} accretion products. The α-pinene system showed a reduction in the fraction of the $C_{10}H_{14}O_z$ family, while the n-dodecane system exhibited a decrease in the fraction of $C_{12}H_{24}O_z$ family. These findings suggest that the RO_2 + RO_2 pathway was suppressed under CO present conditions. In the mixed-precursor systems, the reduction in the fraction of C_{16} to C_{24} accretion products was more moderate, and the contribution of CHON species remained largely unchanged. The fraction of $C_{10}H_{14}O_z$ family decreased, whereas the $C_{12}H_{24}O_z$ family increased. These contrasting changes may suggest that CO suppressed the two precursors to different extents in the mixture, with its influence on n-dodecane being less pronounced than in the single precursor system, thereby resulting in a relatively small overall impact of CO in the mixture.~~

~~These results demonstrate that variations in reaction conditions led to different responses in SOA particle mass yields and composition between the single- and mixed precursor systems, highlighting the need for laboratory experiments conducted under atmospherically relevant conditions.~~

Data availability

All the data in the figures of this study are available upon request to the corresponding authors (g.mcfiggans@manchester.ac.uk and aristeidis.voliotis@manchester.ac.uk)

Author contribution

GX, AV, and GM conceived the study. GX and AV conducted the experiments. AV, TJB, YS, HW, DH provided assistance in instrument operation and data analysis. GX conducted the data analysis and wrote the manuscript with inputs from all the co-authors.

Competing interests

The contact author has declared that none of the authors has any competing interests.

Acknowledgements

Guangzhao Xie acknowledges the joint scholarship of The University of Manchester and Chinese Scholarship Council (CSC) (grant no. 202208330060). Gordon McFiggans acknowledges funding from the Secondary Organic Aerosol Prediction in Realistic Atmospheres (SOAPRA) project (grant no. NE/V012665/1). Aristeidis Voliotis acknowledges funding support from the Natural Environment Research Council (NERC) through the UK National Centre for Atmospheric Science (NCAS). We thank colleagues from the Jülich and Gothenburg teams for valuable discussions, especially Thomas F. Mentel, Mattias

Hallquist, and Sören R. Zorn. We acknowledge the use of ChatGPT (https://chatgpt.com/) for assistance in language refinement of this manuscript.

References

Alfarra, M.R., Hamilton, J.F., Wyche, K.P., Good, N., Ward, M.W., Carr, T., Barley, M.H., Monks, P.S., Jenkin, M.E., Lewis, A.C. and McFiggans, G.B.: The effect of photochemical ageing and initial precursor concentration on the composition and hygroscopic properties of β-caryophyllene secondary organic aerosol, Atmos. Chem. Phys., 12, 6417-6436, http://doi.org/10.5194/acp-12-6417-2012, 2012.

Amedro, D., Miyazaki, K., Parker, A., Schoernaecker, C. and Fittschen, C.: Atmospheric and kinetic studies of OH and HO2 by the FAGE technique, J. Environ. Sci., 24, 78-86, http://doi.org/10.1016/s1001-0742(11)60723-7, 2012.

Andreae, M.O. and Crutzen, P.J.: Atmospheric aerosols: biogeochemical sources and role in atmospheric chemistry, Science, 276, 1052-1058, http://doi.org/10.1126/science.276.5315.1052, 1997.

Atkinson, R.: Atmospheric chemistry of VOCs and NOx, Atmos. Environ., 34, 2063-2101, http://doi.org/10.1016/s1352-2310(99)00460-4, 2000.

Atkinson, R.: Kinetics of the gas-phase reactions of OH radicals with alkanes and cycloalkanes, Atmos. Chem. Phys., 3, 2233-2307, http://doi.org/10.5194/acp-3-2233-2003, 2003.

Atkinson, R.: Rate constants for the atmospheric reactions of alkoxy radicals: An updated estimation method, Atmos. Environ., 41, 8468-8485, http://doi.org/10.1016/j.atmosenv.2007.07.002, 2007.

Atkinson, R. and Arey, J.: Atmospheric Degradation of Volatile Organic Compounds, Chem. Rev., 103, 4605-4638, http://doi.org/10.1021/cr0206420, 2003.

Baker, Y., Kang, S., Wang, H., Wu, R.R., Xu, J., Zanders, A., He, Q.F., Hohaus, T., Ziehm, T., Geretti, V., Bannan, T.J., O'Meara, S.P., Voliotis, A., Hallquist, M., McFiggans, G., Zorn, S.R., Wahner, A. and Mentel, T.F.: Impact of HO2/RO2 ratio on highly oxygenated α-pinene photooxidation products and secondary organic aerosol formation potential, Atmos. Chem. Phys., 24, 4789-4807, http://doi.org/10.5194/acp-24-4789-2024, 2024.

Bannan, T.J., Le Breton, M., Priestley, M., Worrall, S.D., Bacak, A., Marsden, N.A., Mehra, A., Hammes, J., Hallquist, M., Alfarra, M.R., Krieger, U.K., Reid, J.P., Jayne, J., Robinson, W., McFiggans, G., Coe, H., Percival, C.J. and Topping, D.: A method for extracting calibrated volatility information from the FIGAERO-HR-ToF-CIMS and its experimental application, Atmos. Meas. Tech., 12, 1429-1439, http://doi.org/10.5194/amt-12-1429-2019, 2019.

Berndt, T., Richters, S., Jokinen, T., Hyttinen, N., Kurtén, T., Otkjær, R.V., Kjaergaard, H.G., Stratmann, F., Herrmann, H., Sipilä, M., Kulmala, M. and Ehn, M.: Hydroxyl radical-induced formation of highly oxidized organic compounds, Nat. Commun., 7, 13677, http://doi.org/10.1038/ncomms13677, 2016.

Bianchi, F., Kurten, T., Riva, M., Mohr, C., Rissanen, M.P., Roldin, P., Berndt, T., Crounse, J.D., Wennberg, P.O., Mentel, T.F., Wildt, J., Junninen, H., Jokinen, T., Kulmala, M., Worsnop, D.R., Thornton, J.A., Donahue, N., Kjaergaard, H.G. and Ehn, M.: Highly Oxygenated Organic Molecules (HOM) from Gas-Phase Autoxidation Involving Peroxy Radicals: A Key Contributor to Atmospheric Aerosol, Chem. Rev., 119, 3472-3509, http://doi.org/10.1021/acs.chemrev.8b00395, 2019.

Budisulistiorini, S.H., Li, X., Bairai, S.T., Renfro, J., Liu, Y., Liu, Y.J., McKinney, K.A., Martin, S.T., McNeill, V.F., Pye, H.O.T., Nenes, A., Neff, M.E., Stone, E.A., Mueller, S., Knote, C., Shaw, S.L., Zhang, Z., Gold, A. and Surratt, J.D.: Examining the effects of anthropogenic emissions on isoprene-derived secondary organic aerosol formation during the 2013 Southern Oxidant and Aerosol Study (SOAS) at the Look Rock, Tennessee ground site, Atmos. Chem. Phys., 15, 8871-8888,

http://doi.org/10.5194/acp-15-8871-2015, 2015.

Burkholder, J.B., Abbatt, J.P.D., Barnes, I., Roberts, J.M., Melamed, M.L., Ammann, M., Bertram, A.K., Cappa, C.D., Carlton, A.G., Carpenter, L.J., Crowley, J.N., Dubowski, Y., Georges, C., Heard, D.E., Herrmann, H., Keutsch, F.N., Kroll, J.H., McNeill, V.F., Ng, N.L., Nizkorodov, S.A., Orlando, J.J., Percival, C.J., Picquet-Varrault, B., Rudich, Y., Seakins, P.W., Surratt, J.D., Tanimoto, H., Thornton, J.A., Tong, Z., Tyndall, G.S., Wahner, A., Weschler, C.J., Wilson, K.R. and Ziemann, P.J.: The Essential Role for Laboratory Studies in Atmospheric Chemistry, Environ. Sci. Technol., 51, 2519-2528, http://doi.org/10.1021/acs.est.6b04947, 2017.

Canagaratna, M.R., Jayne, J.T., Jimenez, J.L., Allan, J.D., Alfarra, M.R., Zhang, Q., Onasch, T.B., Drewnick, F., Coe, H., Middlebrook, A., Delia, A., Williams, L.R., Trimborn, A.M., Northway, M.J., DeCarlo, P.F., Kolb, C.E., Davidovits, P. and Worsnop, D.R.: Chemical and microphysical characterization of ambient aerosols with the aerodyne aerosol mass spectrometer, Mass Spectrom. Rev., 26, 185-222, http://doi.org/10.1002/mas.20115, 2007.

Chen, T.Z., Zhang, P., Ma, Q.X., Chu, B.W., Liu, J., Ge, Y.L. and He, H.: Smog Chamber Study on the Role of NOx in SOA and O3 Formation from Aromatic Hydrocarbons, Environ. Sci. Technol., http://doi.org/10.1021/acs.est.2c04022, 2022.

Clapp, L.J. and Jenkin, M.E.: Analysis of the relationship between ambient levels Of O3, NO2 and NO as a function of NOχ in the UK, Atmos. Environ., 35, 6391-6405, http://doi.org/10.1016/s1352-2310(01)00378-8, 2001.

Dash, M.R., Balaganesh, M. and Rajakumar, B.: Rate coefficients for the gas-phase reaction of OH radical with α-pinene: an experimental and computational study, Mol. Phys., 112, 1495-1511, http://doi.org/10.1080/00268976.2013.840395, 2014.

Dibble, T.S.: Reactions of the Alkoxy Radicals Formed Following OH-Addition to α-Pinene and β-Pinene. C−C Bond Scission Reactions, J. Am. Chem. Soc., 123, 4228-4234, http://doi.org/10.1021/ja003553i, 2001.

Drewnick, F., Hings, S.S., Alfarra, M.R., Prevot, A.S.H. and Borrmann, S.: Aerosol quantification with the Aerodyne Aerosol Mass Spectrometer: detection limits and ionizer background effects, Atmos. Meas. Tech., 2, 33-46, http://doi.org/10.5194/amt-2-33-2009, 2009.

Ehn, M., Thornton, J.A., Kleist, E., Sipila, M., Junninen, H., Pullinen, I., Springer, M., Rubach, F., Tillmann, R., Lee, B., Lopez-Hilfiker, F., Andres, S., Acir, I.H., Rissanen, M., Jokinen, T., Schobesberger, S., Kangasluoma, J., Kontkanen, J., Nieminen, T., Kurten, T., Nielsen, L.B., Jorgensen, S., Kjaergaard, H.G., Canagaratna, M., Dal Maso, M., Berndt, T., Petaja, T., Wahner, A., Kerminen, V.M., Kulmala, M., Worsnop, D.R., Wildt, J. and Mentel, T.F.: A large source of low-volatility secondary organic aerosol, Nature, 506, 476-+, http://doi.org/10.1038/nature13032, 2014.

Gao, L.Y., Song, J.W., Mohr, C., Huang, W., Vallon, M., Jiang, F., Leisner, T. and Saathoff, H.: Kinetics, SOA yields, and chemical composition of seconaary organic aerosol from β-caryophyllene ozonolysis with and without nitrogen oxides between 213 and 313 K, Atmos. Chem. Phys., 22, 6001-6020, http://doi.org/10.5194/acp-22-6001-2022, 2022.

Goldman, M.J., Green, W.H. and Kroll, J.H.: Chemistry of Simple Organic Peroxy Radicals under Atmospheric through Combustion Conditions: Role of Temperature, Pressure, and NOx Level, J. Phys. Chem. A, 125, 10303-10314, http://doi.org/10.1021/acs.jpca.1c07203, 2021.

Goss, M.B., Kenagy, H.S., Heald, C.L. and Kroll, J.H.: Re-Examining Chemical Conditions of Past Chamber Studies of Secondary Organic Aerosol Formation, ACS ES&T Air, 2, 2117-2130, http://doi.org/10.1021/acsestair.5c00112, 2025.

Gu, S., Guenther, A. and Faiola, C.: Effects of Anthropogenic and Biogenic Volatile Organic Compounds on Los Angeles Air Quality, Environ. Sci. Technol., 55, 12191-12201, http://doi.org/10.1021/acs.est.1c01481, 2021.

Guenther, A., Hewitt, C.N., Erickson, D., Fall, R., Geron, C., Graedel, T., Harley, P., Klinger, L., Lerdau, M., Mckay, W.A., Pierce, T., Scholes, B., Steinbrecher, R., Tallamraju, R., Taylor, J. and Zimmerman, P.: A global model of natural volatile organic compound emissions, J. Geophys. Res., 100, 8873-8892, http://doi.org/10.1029/94JD02950, 1995.

Hallquist, M., Wenger, J.C., Baltensperger, U., Rudich, Y., Simpson, D., Claeys, M., Dommen, J., Donahue, N.M., George, C., Goldstein, A.H., Hamilton, J.F., Herrmann, H., Hoffmann, T., Iinuma, Y., Jang, M., Jenkin, M.E., Jimenez, J.L., Kiendler-Scharr, A., Maenhaut, W., McFiggans, G., Mentel, T.F., Monod, A., Prevot, A.S.H., Seinfeld, J.H., Surratt, J.D., Szmigielski, R. and Wildt, J.: The formation, properties and impact of secondary organic aerosol: current and emerging issues, Atmos. Chem. Phys., 9, 5155-5236, http://doi.org/10.5194/acp-9-5155-2009, 2009.

Jenkin, M.E., Saunders, S.M. and Pilling, M.J.: The tropospheric degradation of volatile organic compounds: a protocol for mechanism development, Atmos. Environ., 31, 81-104, http://doi.org/10.1016/S1352-2310(96)00105-7, 1997.

Jensen, A.R., Koss, A.R., Hales, R.B. and de Gouw, J.A.: Measurements of volatile organic compounds in ambient air by gas-chromatography and real-time Vocus PTR-TOF-MS: calibrations, instrument background corrections, and introducing a PTR Data Toolkit, Atmos. Meas. Tech., 16, 5261-5285, http://doi.org/10.5194/amt-16-5261-2023, 2023.

Jimenez, J.L., Canagaratna, M.R., Donahue, N.M., Prevot, A.S.H., Zhang, Q., Kroll, J.H., DeCarlo, P.F., Allan, J.D., Coe, H., Ng, N.L., Aiken, A.C., Docherty, K.S., Ulbrich, I.M., Grieshop, A.P., Robinson, A.L., Duplissy, J., Smith, J.D., Wilson, K.R., Lanz, V.A., Hueglin, C., Sun, Y.L., Tian, J., Laaksonen, A., Raatikainen, T., Rautiainen, J., Vaattovaara, P., Ehn, M., Kulmala, M., Tomlinson, J.M., Collins, D.R., Cubison, M.J., Dunlea, E.J., Huffman, J.A., Onasch, T.B., Alfarra, M.R., Williams, P.I., Bower, K., Kondo, Y., Schneider, J., Drewnick, F., Borrmann, S., Weimer, S., Demerjian, K., Salcedo, D., Cottrell, L., Griffin, R., Takami, A., Miyoshi, T., Hatakeyama, S., Shimono, A., Sun, J.Y., Zhang, Y.M., Dzepina, K., Kimmel, J.R., Sueper, D., Jayne, J.T., Herndon, S.C., Trimborn, A.M., Williams, L.R., Wood, E.C., Middlebrook, A.M., Kolb, C.E., Baltensperger, U. and Worsnop, D.R.: Evolution of Organic Aerosols in the Atmosphere, Science, 326, 1525-1529, http://doi.org/10.1126/science.1180353, 2009.

Johnson, D. and Marston, G.: The gas-phase ozonolysis of unsaturated volatile organic compounds in the troposphere, Chem. Soc. Rev., 37, 699-716, http://doi.org/10.1039/B704260B, 2008.

Kanakidou, M., Seinfeld, J.H., Pandis, S.N., Barnes, I., Dentener, F.J., Facchini, M.C., Van Dingenen, R., Ervens, B., Nenes, A., Nielsen, C.J., Swietlicki, E., Putaud, J.P., Balkanski, Y., Fuzzi, S., Horth, J., Moortgat, G.K., Winterhalter, R., Myhre, C.E.L., Tsigaridis, K., Vignati, E., Stephanou, E.G. and Wilson, J.: Organic aerosol and global climate modelling: a review, Atmos. Chem. Phys., 5, 1053-1123, http://doi.org/10.5194/acp-5-1053-2005, 2005.

Kang, S., Wildt, J., Pullinen, I., Vereecken, L., Wu, C., Wahner, A., Zorn, S.R. and Mentel, T.F.: Formation of highly oxygenated organic molecules from α-pinene photooxidation: evidence for the importance of highly oxygenated alkoxy radicals, Atmos. Chem. Phys., 25, 15715-15740, http://doi.org/10.5194/acp-25-15715-2025, 2025.

Kenagy, H.S., Heald, C.L., Tahsini, N., Goss, M.B. and Kroll, J.H.: Can we achieve atmospheric chemical environments in the laboratory? An integrated model-measurement approach to chamber SOA studies, Sci. Adv., 10, eado1482, http://doi.org/doi:10.1126/sciadv.ado1482, 2024.

Kiendler-Scharr, A., Mensah, A.A., Friese, E., Topping, D., Nemitz, E., Prevot, A.S.H., Äijälä, M., Allan, J., Canonaco, F., Canagaratna, M., Carbone, S., Crippa, M., Dall Osto, M., Day, D.A., De Carlo, P., Di Marco, C.F., Elbern, H., Eriksson, A., Freney, E., Hao, L., Herrmann, H., Hildebrandt, L., Hillamo, R., Jimenez, J.L., Laaksonen, A., McFiggans, G., Mohr, C.,

O'Dowd, C., Otjes, R., Ovadnevaite, J., Pandis, S.N., Poulain, L., Schlag, P., Sellegri, K., Swietlicki, E., Tiitta, P., Vermeulen, A., Wahner, A., Worsnop, D. and Wu, H.-C.: Ubiquity of organic nitrates from nighttime chemistry in the European submicron aerosol, Geophys. Res. Lett., 43, 7735-7744, http://doi.org/10.1002/2016GL069239, 2016.

Krechmer, J., Lopez-Hilfiker, F., Koss, A., Hutterli, M., Stoermer, C., Deming, B., Kimmel, J., Warneke, C., Holzinger, R., Jayne, J., Worsnop, D., Fuhrer, K., Gonin, M. and de Gouw, J.: Evaluation of a New Reagent-Ion Source and Focusing Ion–Molecule Reactor for Use in Proton-Transfer-Reaction Mass Spectrometry, Anal. Chem., 90, 12011-12018, http://doi.org/10.1021/acs.analchem.8b02641, 2018.

Kroll, J.H. and Seinfeld, J.H.: Chemistry of secondary organic aerosol: Formation and evolution of low-volatility organics in the atmosphere, Atmos. Environ., 42, 3593-3624, http://doi.org/10.1016/j.atmosenv.2008.01.003, 2008.

Lane, T.E., Donahue, N.M. and Pandis, S.N.: Effect of NOx on Secondary Organic Aerosol Concentrations, Environ. Sci. Technol., 42, 6022-6027, http://doi.org/10.1021/es703225a, 2008.

Lannuque, V., D'Anna, B., Kostenidou, E., Couvidat, F., Martinez-Valiente, A., Eichler, P., Wisthaler, A., Müller, M., Temime-Roussel, B., Valorso, R. and Sartelet, K.: Gas–particle partitioning of toluene oxidation products: an experimental and modeling study, Atmos. Chem. Phys., 23, 15537-15560, http://doi.org/10.5194/acp-23-15537-2023, 2023.

Lee, A., Goldstein, A.H., Kroll, J.H., Ng, N.L., Varutbangkul, V., Flagan, R.C. and Seinfeld, J.H.: Gas-phase products and secondary aerosol yields from the photooxidation of 16 different terpenes, J. Geophys. Res. Atmos., 111, http://doi.org/10.1029/2006jd007050, 2006.

Lee, B.H., Lopez-Hilfiker, F.D., Mohr, C., Kurtén, T., Worsnop, D.R. and Thornton, J.A.: An Iodide-Adduct High-Resolution Time-of-Flight Chemical-Ionization Mass Spectrometer: Application to Atmospheric Inorganic and Organic Compounds, Environ. Sci. Technol., 48, 6309-6317, http://doi.org/10.1021/es500362a, 2014.

Lopez-Hilfiker, F.D., Mohr, C., Ehn, M., Rubach, F., Kleist, E., Wildt, J., Mentel, T.F., Lutz, A., Hallquist, M., Worsnop, D. and Thornton, J.A.: A novel method for online analysis of gas and particle composition: description and evaluation of a Filter Inlet for Gases and AEROsols (FIGAERO), Atmos. Meas. Tech., 7, 983-1001, http://doi.org/10.5194/amt-7-983-2014, 2014.

Lu, Y. and Khalil, M.A.K.: Methane and carbon-monoxide in OH chemistry - The effects of feedbacks and reservoirs generated by the reactive products, Chemosphere, 26, 641-655, http://doi.org/10.1016/0045-6535(93)90450-j, 1993.

McFiggans, G., Mentel, T.F., Wildt, J., Pullinen, I., Kang, S., Kleist, E., Schmitt, S., Springer, M., Tillmann, R., Wu, C., Zhao, D.F., Hallquist, M., Faxon, C., Le Breton, M., Hallquist, A.M., Simpson, D., Bergstrom, R., Jenkin, M.E., Ehn, M., Thornton, J.A., Alfarra, M.R., Bannan, T.J., Percival, C.J., Priestley, M., Topping, D. and Kiendler-Scharr, A.: Secondary organic aerosol reduced by mixture of atmospheric vapours, Nature, 565, 587-593, http://doi.org/10.1038/s41586-018-0871-y, 2019.

Molteni, U., Simon, M., Heinritzi, M., Hoyle, C.R., Bernhammer, A.-K., Bianchi, F., Breitenlechner, M., Brilke, S., Dias, A., Duplissy, J., Frege, C., Gordon, H., Heyn, C., Jokinen, T., Kürten, A., Lehtipalo, K., Makhmutov, V., Petäjä, T., Pieber, S.M., Praplan, A.P., Schobesberger, S., Steiner, G., Stozhkov, Y., Tomé, A., Tröstl, J., Wagner, A.C., Wagner, R., Williamson, C., Yan, C., Baltensperger, U., Curtius, J., Donahue, N.M., Hansel, A., Kirkby, J., Kulmala, M., Worsnop, D.R. and Dommen, J.: Formation of Highly Oxygenated Organic Molecules from α-Pinene Ozonolysis: Chemical Characteristics, Mechanism, and Kinetic Model Development, ACS Earth Space Chem., 3, 873-883, http://doi.org/10.1021/acsearthspacechem.9b00035, 2019.

Nah, T., McVay, R.C., Pierce, J.R., Seinfeld, J.H. and Ng, N.L.: Constraining uncertainties in particle-wall deposition correction during SOA formation in chamber experiments, Atmos. Chem. Phys., 17, 2297-2310, http://doi.org/10.5194/acp-

17-2297-2017, 2017.

Okada, Y., Nakagoshi, A., Tsurukawa, M., Matsumura, C., Eiho, J. and Nakano, T.: Environmental risk assessment and concentration trend of atmospheric volatile organic compounds in Hyogo Prefecture, Japan, Environ. Sci. Pollut. Res., 19, 201-213, http://doi.org/10.1007/s11356-011-0550-0, 2012.

Orlando, J.J., Tyndall, G.S. and Wallington, T.J.: The Atmospheric Chemistry of Alkoxy Radicals, Chem. Rev., 103, 4657-4690, http://doi.org/10.1021/cr020527p, 2003.

Peräkylä, O., Berndt, T., Franzon, L., Hasan, G., Meder, M., Valiev, R.R., Daub, C.D., Varelas, J.G., Geiger, F.M., Thomson, R.J., Rissanen, M., Kurtén, T. and Ehn, M.: Large Gas-Phase Source of Esters and Other Accretion Products in the Atmosphere, J. Am. Chem. Soc., 145, 7780-7790, http://doi.org/10.1021/jacs.2c10398, 2023.

Pospisilova, V., Lopez-Hilfiker, F.D., Bell, D.M., El Haddad, I., Mohr, C., Huang, W., Heikkinen, L., Xiao, M., Dommen, J., Prevot, A.S.H., Baltensperger, U. and Slowik, J.G.: On the fate of oxygenated organic molecules in atmospheric aerosol particles, Sci. Adv., 6, eaax8922, http://doi.org/doi:10.1126/sciadv.aax8922, 2020.

Presto, A.A., Huff Hartz, K.E. and Donahue, N.M.: Secondary Organic Aerosol Production from Terpene Ozonolysis. 1. Effect of UV Radiation, Environ. Sci. Technol., 39, 7036-7045, http://doi.org/10.1021/es050174m, 2005.

Pullinen, I., Schmitt, S., Kang, S., Sarrafzadeh, M., Schlag, P., Andres, S., Kleist, E., Mentel, T.F., Rohrer, F., Springer, M., Tillmann, R., Wildt, J., Wu, C., Zhao, D., Wahner, A. and Kiendler-Scharr, A.: Impact of NOx on secondary organic aerosol (SOA) formation from α-pinene and β-pinene photooxidation: the role of highly oxygenated organic nitrates, Atmos. Chem. Phys., 20, 10125-10147, http://doi.org/10.5194/acp-20-10125-2020, 2020.

Pusede, S.E., Steiner, A.L. and Cohen, R.C.: Temperature and Recent Trends in the Chemistry of Continental Surface Ozone, Chem. Rev., 115, 3898-3918, http://doi.org/10.1021/cr5006815, 2015.

Pye, H.O.T., D'Ambro, E.L., Lee, B.H., Schobesberger, S., Takeuchi, M., Zhao, Y., Lopez-Hilfiker, F., Liu, J., Shilling, J.E., Xing, J., Mathur, R., Middlebrook, A.M., Liao, J., Welti, A., Graus, M., Warneke, C., de Gouw, J.A., Holloway, J.S., Ryerson, T.B., Pollack, I.B. and Thornton, J.A.: Anthropogenic enhancements to production of highly oxygenated molecules from autoxidation, Proc. Natl. Acad. Sci. U.S.A., 116, 6641-6646, http://doi.org/doi:10.1073/pnas.1810774116, 2019.

Ramanathan, V., Crutzen, P.J., Kiehl, J.T. and Rosenfeld, D.: Atmosphere - Aerosols, climate, and the hydrological cycle, Science, 294, 2119-2124, http://doi.org/10.1126/science.1064034, 2001.

Robinson, A.L., Donahue, N.M., Shrivastava, M.K., Weitkamp, E.A., Sage, A.M., Grieshop, A.P., Lane, T.E., Pierce, J.R. and Pandis, S.N.: Rethinking organic aerosols: Semivolatile emissions and photochemical aging, Science, 315, 1259-1262, http://doi.org/10.1126/science.1133061, 2007.

Sarrafzadeh, M., Wildt, J., Pullinen, I., Springer, M., Kleist, E., Tillmann, R., Schmitt, S.H., Wu, C., Mentel, T.F., Zhao, D., Hastie, D.R. and Kiendler-Scharr, A.: Impact of NOx and OH on secondary organic aerosol formation from β-pinene photooxidation, Atmos. Chem. Phys., 16, 11237-11248, http://doi.org/10.5194/acp-16-11237-2016, 2016.

Shao, Y.Q., Wang, Y., Du, M., Voliotis, A., Alfarra, M.R., O'Meara, S.P., Turner, S.F. and McFiggans, G.: Characterisation of the Manchester Aerosol Chamber facility, Atmos. Meas. Tech., 15, 539-559, http://doi.org/10.5194/amt-15-539-2022, 2022.

Shilling, J.E., Zaveri, R.A., Fast, J.D., Kleinman, L., Alexander, M.L., Canagaratna, M.R., Fortner, E., Hubbe, J.M., Jayne, J.T., Sedlacek, A., Setyan, A., Springston, S., Worsnop, D.R. and Zhang, Q.: Enhanced SOA formation from mixed anthropogenic and biogenic emissions during the CARES campaign, Atmos. Chem. Phys., 13, 2091-2113,

http://doi.org/10.5194/acp-13-2091-2013, 2013.

Shrivastava, M., Cappa, C.D., Fan, J.W., Goldstein, A.H., Guenther, A.B., Jimenez, J.L., Kuang, C., Laskin, A., Martin, S.T., Ng, N.L., Petaja, T., Pierce, J.R., Rasch, P.J., Roldin, P., Seinfeld, J.H., Shilling, J., Smith, J.N., Thornton, J.A., Volkamer, R., Wang, J., Worsnop, D.R., Zaveri, R.A., Zelenyuk, A. and Zhang, Q.: Recent advances in understanding secondary organic aerosol: Implications for global climate forcing, Rev. Geophys., 55, 509-559, http://doi.org/10.1002/2016rg000540, 2017.

Srivastava, D., Vu, T.V., Tong, S., Shi, Z. and Harrison, R.M.: Formation of secondary organic aerosols from anthropogenic precursors in laboratory studies, npj Clim. Atmos. Sci., 5, 22, http://doi.org/10.1038/s41612-022-00238-6, 2022.

Stone, E.A., Hedman, C.J., Zhou, J., Mieritz, M. and Schauer, J.J.: Insights into the nature of secondary organic aerosol in Mexico City during the MILAGRO experiment 2006, Atmos. Environ., 44, 312-319, http://doi.org/10.1016/j.atmosenv.2009.10.036, 2010.

Takeuchi, M., Berkemeier, T., Eris, G. and Ng, N.L.: Non-linear effects of secondary organic aerosol formation and properties in multi-precursor systems, Nat. Commun., 13, http://doi.org/10.1038/s41467-022-35546-1, 2022.

Tsigaridis, K., Daskalakis, N., Kanakidou, M., Adams, P.J., Artaxo, P., Bahadur, R., Balkanski, Y., Bauer, S.E., Bellouin, N., Benedetti, A., Bergman, T., Berntsen, T.K., Beukes, J.P., Bian, H., Carslaw, K.S., Chin, M., Curci, G., Diehl, T., Easter, R.C., Ghan, S.J., Gong, S.L., Hodzic, A., Hoyle, C.R., Iversen, T., Jathar, S., Jimenez, J.L., Kaiser, J.W., Kirkevåg, A., Koch, D., Kokkola, H., Lee, Y.H., Lin, G., Liu, X., Luo, G., Ma, X., Mann, G.W., Mihalopoulos, N., Morcrette, J.J., Müller, J.F., Myhre, G., Myriokefalitakis, S., Ng, N.L., O'Donnell, D., Penner, J.E., Pozzoli, L., Pringle, K.J., Russell, L.M., Schulz, M., Sciare, J., Seland, O., Shindell, D.T., Sillman, S., Skeie, R.B., Spracklen, D., Stavrakou, T., Steenrod, S.D., Takemura, T., Tiitta, P., Tilmes, S., Tost, H., van Noije, T., van Zyl, P.G., von Salzen, K., Yu, F., Wang, Z., Wang, Z., Zaveri, R.A., Zhang, H., Zhang, K., Zhang, Q. and Zhang, X.: The AeroCom evaluation and intercomparison of organic aerosol in global models, Atmos. Chem. Phys., 14, 10845-10895, http://doi.org/10.5194/acp-14-10845-2014, 2014.

Vereecken, L. and Peeters, J.: Nontraditional (Per)oxy Ring-Closure Paths in the Atmospheric Oxidation of Isoprene and Monoterpenes, J. Phys. Chem. A, 108, 5197-5204, http://doi.org/10.1021/jp049219g, 2004.

Voliotis, A., Du, M., Wang, Y., Shao, Y.Q., Alfarra, M.R., Bannan, T.J., Hu, D.W., Pereira, K.L., Hamilton, J.F., Hallquist, M., Mentel, T.F. and McFiggans, G.: Chamber investigation of the formation and transformation of secondary organic aerosol in mixtures of biogenic and anthropogenic volatile organic compounds, Atmos. Chem. Phys., 22, 14147-14175, http://doi.org/10.5194/acp-22-14147-2022, 2022a.

Voliotis, A., Du, M., Wang, Y., Shao, Y.Q., Bannan, T.J., Flynn, M., Pandis, S.N., Percival, C.J., Alfarra, M.R. and McFiggans, G.: The influence of the addition of isoprene on the volatility of particles formed from the photo-oxidation of anthropogenic-biogenic mixtures, Atmos. Chem. Phys., 22, 13677-13693, http://doi.org/10.5194/acp-22-13677-2022, 2022b.

Voliotis, A., Wang, Y., Shao, Y.Q., Du, M., Bannan, T.J., Percival, C.J., Pandis, S.N., Alfarra, M.R. and McFiggans, G.: Exploring the composition and volatility of secondary organic aerosols in mixed anthropogenic and biogenic precursor systems, Atmos. Chem. Phys., 21, 14251-14273, http://doi.org/10.5194/acp-21-14251-2021, 2021.

Volkamer, R., Jimenez, J.L., San Martini, F., Dzepina, K., Zhang, Q., Salcedo, D., Molina, L.T., Worsnop, D.R. and Molina, M.J.: Secondary organic aerosol formation from anthropogenic air pollution: Rapid and higher than expected, Geophys. Res. Lett., 33, http://doi.org/10.1029/2006GL026899, 2006.

Wang, N.X., Jorga, S.D., Pierce, J.R., Donahue, N.M. and Pandis, S.N.: Particle wall-loss correction methods in smog chamber

experiments, Atmos. Meas. Tech., 11, 6577-6588, http://doi.org/10.5194/amt-11-6577-2018, 2018.

Xu, L., Guo, H., Boyd, C.M., Klein, M., Bougiatioti, A., Cerully, K.M., Hite, J.R., Isaacman-VanWertz, G., Kreisberg, N.M., Knote, C., Olson, K., Koss, A., Goldstein, A.H., Hering, S.V., de Gouw, J., Baumann, K., Lee, S.-H., Nenes, A., Weber, R.J. and Ng, N.L.: Effects of anthropogenic emissions on aerosol formation from isoprene and monoterpenes in the southeastern United States, Proc. Natl. Acad. Sci. U.S.A., 112, 37-42, http://doi.org/doi:10.1073/pnas.1417609112, 2015.

Yuan, B., Koss, A.R., Warneke, C., Coggon, M., Sekimoto, K. and de Gouw, J.A.: Proton-Transfer-Reaction Mass Spectrometry: Applications in Atmospheric Sciences, Chem. Rev., 117, 13187-13229, http://doi.org/10.1021/acs.chemrev.7b00325, 2017.

Zhang, X., Schwantes, R.H., Coggon, M.M., Loza, C.L., Schilling, K.A., Flagan, R.C. and Seinfeld, J.H.: Role of ozone in SOA formation from alkane photooxidation, Atmos. Chem. Phys., 14, 1733-1753, http://doi.org/10.5194/acp-14-1733-2014, 2014.

Zhao, D.F., Schmitt, S.H., Wang, M.J., Acir, I.H., Tillmann, R., Tan, Z.F., Novelli, A., Fuchs, H., Pullinen, I., Wegener, R., Rohrer, F., Wildt, J., Kiendler-Scharr, A., Wahner, A. and Mentel, T.F.: Effects of NOx and SO2 on the secondary organic aerosol formation from photooxidation of α-pinene and limonene, Atmos. Chem. Phys., 18, 1611-1628, http://doi.org/10.5194/acp-18-1611-2018, 2018.

Zhao, Y.L., Nguyen, N.T., Presto, A.A., Hennigan, C.J., May, A.A. and Robinson, A.L.: Intermediate Volatility Organic Compound Emissions from On-Road Diesel Vehicles: Chemical Composition, Emission Factors, and Estimated Secondary Organic Aerosol Production, Environ. Sci. Technol., 49, 11516-11526, http://doi.org/10.1021/acs.est.5b02841, 2015.

Zhou, C.F., Jang, M. and Yu, Z.C.: Simulation of SOA formation from the photooxidation of monoalkylbenzenes in the presence of aqueous aerosols containing electrolytes under various NOx levels, Atmos. Chem. Phys., 19, 5719-5735, http://doi.org/10.5194/acp-19-5719-2019, 2019.

Ziemann, P.J. and Atkinson, R.: Kinetics, products, and mechanisms of secondary organic aerosol formation, Chem. Soc. Rev., 41, 6582-6605, http://doi.org/10.1039/c2cs35122f, 2012.